Cell Reports
Medicine

Article

Activation of hepatic adenosine A1 receptor ameliorates MASH via inhibiting SREBPs maturation

Graphical abstract

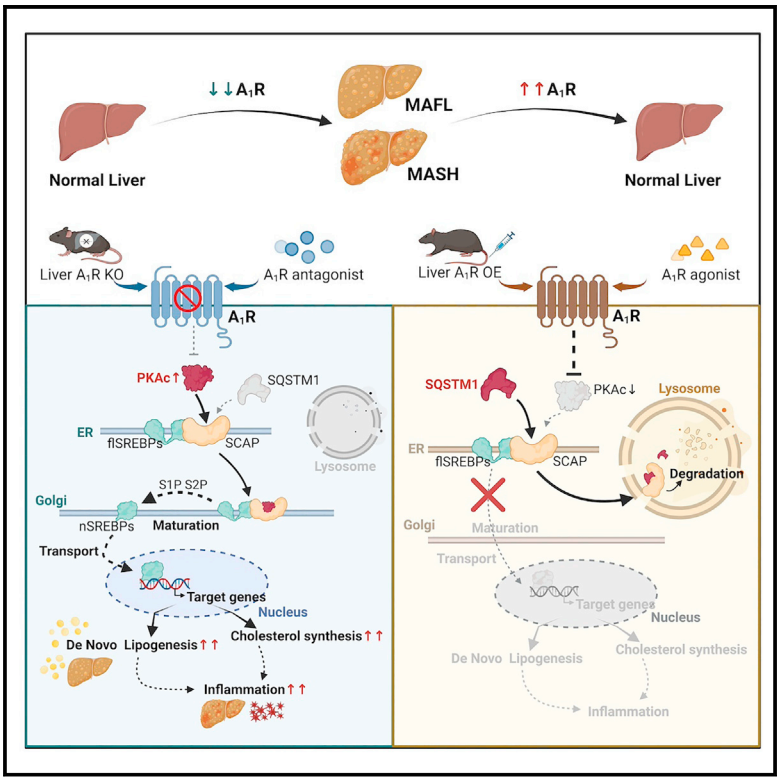

Highlights

- Hepatic A_1R activation ameliorates MAFL and MASH in mice
- Activated hepatic A_1R reduces *de novo* lipogenesis via inhibiting SREBP maturation
- Activated hepatic A_1R promotes the binding of SQSTM1 to SCAP, leading to SCAP degradation
- Hepatic A_1R is a potential therapeutic target for MASH

Authors

Weize Zhu, Ying Hong, Zhaowei Tong, ..., Jing Zhong, Lili Sheng, Houkai Li

Correspondence

mingxiaoli0928@126.com (M.L.), Zhongjing1003@126.com (J.Z.), llsheng@shutcm.edu.cn (L.S.), hk_li@shutcm.edu.cn (H.L.)

In brief

Zhu et al. show that hepatic A_1R activation reduces the direct binding of SCAP with PKAc but increases the formation of an SCAP-SQSTM1 complex, facilitating SCAP degradation in the lysosome, and suppressing the maturation of SREBPs. Hepatic A_1R is a promising target for MAFLD therapy.

Zhu et al., 2024, Cell Reports Medicine *5*, 101477
March 19, 2024
https://doi.org/10.1016/j.xcrm.2024.101477

CellPress

Cell Reports Medicine

CellPress
OPEN ACCESS

Article

Activation of hepatic adenosine A1 receptor ameliorates MASH via inhibiting SREBPs maturation

Weize Zhu,[1,9] Ying Hong,[1,9] Zhaowei Tong,[2] Xiaofang He,[1] Yan Li,[1] Hao Wang,[1] Xinxin Gao,[1] Pengtao Song,[3] Xianshan Zhang,[2] Xiaochang Wu,[4] Zhenhua Tan,[4] Wenjin Huang,[1] Zekun Liu,[1] Yiyang Bao,[1] Junli Ma,[1] Ningning Zheng,[1] Cen Xie,[5] Xisong Ke,[6] Wen Zhou,[7] Wei Jia,[8] Mingxiao Li,[1,*] Jing Zhong,[2,*] Lili Sheng,[1,*] and Houkai Li[1,10,*]

[1]School of Pharmacy, Shanghai University of Traditional Chinese Medicine, Shanghai 201203, China
[2]Huzhou Key Laboratory of Precision Medicine Research and Translation for Infectious Diseases, Huzhou Central Hospital, Affiliated Central Hospital Huzhou University, Huzhou 313000, China
[3]Department of Pathology, Huzhou Central Hospital, Affiliated Central Hospital Huzhou University, Huzhou 313000, China
[4]Department of Hepatobiliary Surgery, Huzhou Central Hospital, Affiliated Central Hospital Huzhou University, Huzhou 313000, China
[5]Shanghai Frontiers Science Center of TCM Chemical Biology, Institute of Interdisciplinary Integrative Medicine Research, Shanghai University of Traditional Chinese Medicine, Shanghai 201203, China
[6]State Key Laboratory of Drug Research, Shanghai Institute of Materia Medica, Chinese Academy of Sciences, Shanghai 201203, China
[7]Key Laboratory of Veterinary Chemical Drugs and Pharmaceutics, Ministry of Agriculture and Rural, Affairs, Shanghai Veterinary Research Institute, Chinese Academy of Agricultural Sciences, Shanghai 200241, China
[8]School of Chinese Medicine, Hong Kong Baptist University, Kowloon Tong, Hong Kong 999077, China
[9]These authors contributed equally
[10]Lead contact
*Correspondence: mingxiaoli0928@126.com (M.L.), Zhongjing1003@126.com (J.Z.), llsheng@shutcm.edu.cn (L.S.), hk_li@shutcm.edu.cn (H.L.)
https://doi.org/10.1016/j.xcrm.2024.101477

SUMMARY

Metabolic (dysfunction)-associated steatohepatitis (MASH) is the advanced stage of metabolic (dysfunction)-associated fatty liver disease (MAFLD) lacking approved clinical drugs. Adenosine A1 receptor (A_1R), belonging to the G-protein-coupled receptors (GPCRs) superfamily, is mainly distributed in the central nervous system and major peripheral organs with wide-ranging physiological functions; however, the exact role of hepatic A_1R in MAFLD remains unclear. Here, we report that liver-specific depletion of A_1R aggravates while overexpression attenuates diet-induced metabolic-associated fatty liver (MAFL)/MASH in mice. Mechanistically, activation of hepatic A_1R promotes the competitive binding of sterol-regulatory element binding protein (SREBP) cleavage-activating protein (SCAP) to sequestosome 1 (SQSTM1), rather than protein kinase A (PKA) leading to SCAP degradation in lysosomes. Reduced SCAP hinders SREBP1c/2 maturation and thus suppresses *de novo* lipogenesis and inflammation. Higher hepatic A_1R expression is observed in patients with MAFL/MASH and high-fat diet (HFD)-fed mice, which is supposed to be a physiologically adaptive response because A_1R agonists attenuate MAFL/MASH in an A_1R-dependent manner. These results highlight that hepatic A_1R is a potential target for MAFL/MASH therapy.

INTRODUCTION

Metabolic (dysfunction)-associated fatty liver disease (MAFLD) was formerly known as nonalcoholic fatty liver disease (NAFLD)[1–4] and is the predominant chronic liver disease with a broad spectrum consisting of steatosis (fatty liver [MAFL]), steatohepatitis (metabolic-associate steatohepatitis [MASH]), fibrosis, cirrhosis, and hepatocellular carcinoma (HCC).[5,6] Although MAFL is the early and reversible stage of MAFLD, some MAFL patients will progress to MASH and even irreversible advanced stages.[7,8] To date, there are no approved drugs for MASH therapy in clinic. Therefore, the identification of novel therapeutic targets of MASH is urgently needed.

Adenosine receptor (AR) belongs to the G-protein-coupled receptor (GPCR) superfamily, consisting of A_1R, $A_{2A}R$, $A_{2B}R$, and A_3R subtypes, which are widely distributed in central nervous system and major peripheral organs with different abundance.[9] ARs are activated upon extracellular adenosine that derives from ATP/ADP hydrolysis catalyzed by CD39 and CD73. The CD39/CD73-adenosine-ARs axis is implicated in immune and inflammation-related diseases where the increased inflammation and cellular hypoxia stimulate the generation of adenosine, resulting in diversified outcomes depending on the activated subtype of ARs and cellular distribution.[10,11] Recent study reveals that $A_{2A}R$ is a novel tumor suppressor of MASH-associated HCC[12] and antagonism of $A_{2A}R$ enhances immunotherapy efficacy.[13,14] $A_{2B}R$ has been implicated in regulatory T cell functions and is a contributing factor in adenosine-mediated protection against inflammatory disease and organ injury.[15,16] A_3R is involved in the inhibition of neutrophil degranulation in tissue

injury,[17] and activation of A_3R reverses neuropathic pain via T cell-mediated production of interleukin (IL)-10.[18] A_1R is highly expressed in central nervous system, heart atria, kidney, pancreas, adipose tissue, etc.[9,19] Therefore, A_1R is a potential therapeutic target for diseases such as Parkinsonism, Alzheimer's disease, diabetes, and obesity,[20–23] and several specific agonists or antagonists of A_1R are under phase II/III trials.[24–26]

In contrast to the well-established distribution and role of A_1R in central nervous system and other peripheral organs,[9] hepatic A_1R expression is supposed to be weak in liver under physiological condition.[27] Nevertheless, studies suggested that dysregulated hepatic A_1R signaling was associated with some liver diseases, such as liver fibrosis, hepatic ischemia-reperfusion injury, and intrahepatic cholestasis.[28–30] Notably, it was reported that global A_1R knockout mice were resistant to alcohol-induced liver disease, and the underlying mechanism was supposed to be associated with the suppression of sterol-regulatory element binding protein 1c (SREBP1c)-mediated fatty acid *de novo* lipogenesis (DNL).[31] However, this effect was not consistently observed in another study, which was supposed to be due to the low expression of A_1R in hepatocytes.[27] Paradoxically, the presence of the four subtypes of ARs in hepatocytes in either human beings or rodents has also been demonstrated, with the A_1R sequence being the most conserved.[9,32] Thus, the exact role of hepatic A_1R in MAFLD development and progression remains uncertain.

In this study, we first investigated the role of hepatic A_1R by generating liver-specific A_1R knockout ($A_1R^{Liver-/-}$) and overexpressed ($A_1R^{Liver\ OE}$) mice in high-fat diet (HFD) and choline-deficient (CD)-HFD-induced MAFL and MASH models. Liver-specific deletion of A_1R aggregated diet-induced MAFL or MASH, which was attenuated in $A_1R^{Liver\ OE}$ mice. Mechanistically, our results revealed that activated A_1R suppressed the maturation of SREBPs (SREBP1c/2), leading to the inhibition of DNL via protein kinase A catalytic subunit (PKAc)/SREBP cleavage-activating protein (SCAP) pathway. Activated A_1R accelerated the degradation of SCAP protein in lysosome and reduced its anchoring at Golgi apparatus by forming SCAP-sequestosome 1 (SQSTM1) complex. Ultimately, we demonstrated that activation of hepatic A_1R by pharmacological agonist 2-chloro-N^6-cyclopentyladenosine (CCPA) or screened natural compound timosaponin AIII (TA3) with potent activating ability on A_1R ameliorated diet-induced MAFL and MASH in mice in an A_1R-dependent manner. Our current findings revealed a previously undetermined role of hepatic A_1R as a promising therapeutic target for MAFL and MASH.

RESULTS

Liver-specific A_1R knockout exaggerates MAFL and MASH in mice

To investigate the exact role of hepatic A_1R in MAFLD formation, we first generated liver-specific A_1R knockout (LKO) mice with no impact on the expression of other AR subtypes (Figures S1A–S1D). In the context of the normal chow diet (NCD), liver-specific A_1R deletion did not affect body weight gain, liver function, or histology (Figures S1E–S1H). Nevertheless, NCD-fed LKO mice showed increased hepatocyte triglyceride (TG), impaired glucose tolerance, and elevated protein expression of fatty acid synthase (FASN) and acetyl-coenzyme A (CoA) carboxylase (ACC) (Figures S1I–S1K), implying that liver-specific A_1R ablation might activate hepatic DNL. Then, we observed that liver-specific ablation of A_1R aggravated hepatic steatosis, increased liver index and serum alanine aminotransferase (ALT) level, induced dyslipidemia, and impaired glucose homeostasis in HFD-induced MAFL mice (Figures 1A–1E and S1L–S1S). Meanwhile, LKO mice showed increased liver pro-inflammatory cytokine (IL-β, tumor necrosis factor [TNF]-α) levels and enhanced protein expression of hepatic FASN and ACC but not CPT1α or CD36 (Figures S1T and 1F).

To test whether liver-specific ablation of A_1R would aggravate MASH formation, we fed mice with CD-HFD, a commonly used diet for inducing a MASH model in relatively short time[33] (Figure 1G). Histopathological examination revealed elevated hepatic steatosis, fibrosis, macrophage marker F4/80 and CD11b, and NAFLD activity score (NAS) in LKO mice (Figures 1H and S1U). These changes were accompanied with increased serum ALT and aspartate transaminase (AST) activities and serum inflammatory cytokines (IL-1β, IL-6, and TNF-α), as well as increased gene expression of fibrosis markers, chemotactic factors, and inflammatory cytokines, suggesting enhanced liver damage and inflammation (Figures 1I, 1J, and S1V). The liver TG of LKO mice on CD-HFD was higher than Flox mice (Figure 1K). In addition, elevated protein expression of myofibroblast markers alpha smooth muscle actin (α-SMA) and inflammation pathway phosphorylated P65[34] but reduced IκB[35] level were also observed in LKO mice (Figure 1L). We also measured the expression of TGF-β and phosphorylated Smad2 (p-Smad2)/Smad2 that are critically involved in fibrosis development.[36] Our results showed that hepatic A_1R knockout enhanced the expression of TGFβ and the phosphorylation of Smad2 (Figure S1W). Quantification of ^{13}C-incorporated fatty acids was conducted with liver tissue of mice in the context of short-term amylin liver NASH (AMLN) diet feeding. The results showed DNL was obviously higher in LKO than Flox mice (Figure S1X), which consolidated the observation of increased DNL in hepatic A_1R deletion mice. These results indicated that absence of hepatic A_1R exaggerated the diet-induced MAFL and MASH in mice.

Liver-specific A_1R overexpression protects mice from MAFL and MASH

The physiological role of hepatic A_1R was further validated by adeno-associated virus (AAV)-mediated liver-specific A_1R overexpression in mice ($A_1R^{Liver\ OE}$, Figure S2A). In contrast to the observations in LKO mice, $A_1R^{Liver\ OE}$ mice showed dramatic improvements in HFD-induced metabolic disorders including reduced hepatic steatosis and dyslipidemia, improved liver function, and glucose homeostasis (Figures 2A–2E and S2A–S2H). In addition, $A_1R^{Liver\ OE}$ mice also showed decreased hepatic inflammatory cytokines, including IL-1β, IL-6, and TNF-α (Figure S2I). Moreover, overexpression of hepatic A_1R significantly suppressed CD36, FASN, and ACC protein expression (Figure 2F). In line with the protection on MAFL in wild-type (WT) C57BL/6J mice, the protective effect of hepatic A_1R on MAFL

CellPress
OPEN ACCESS

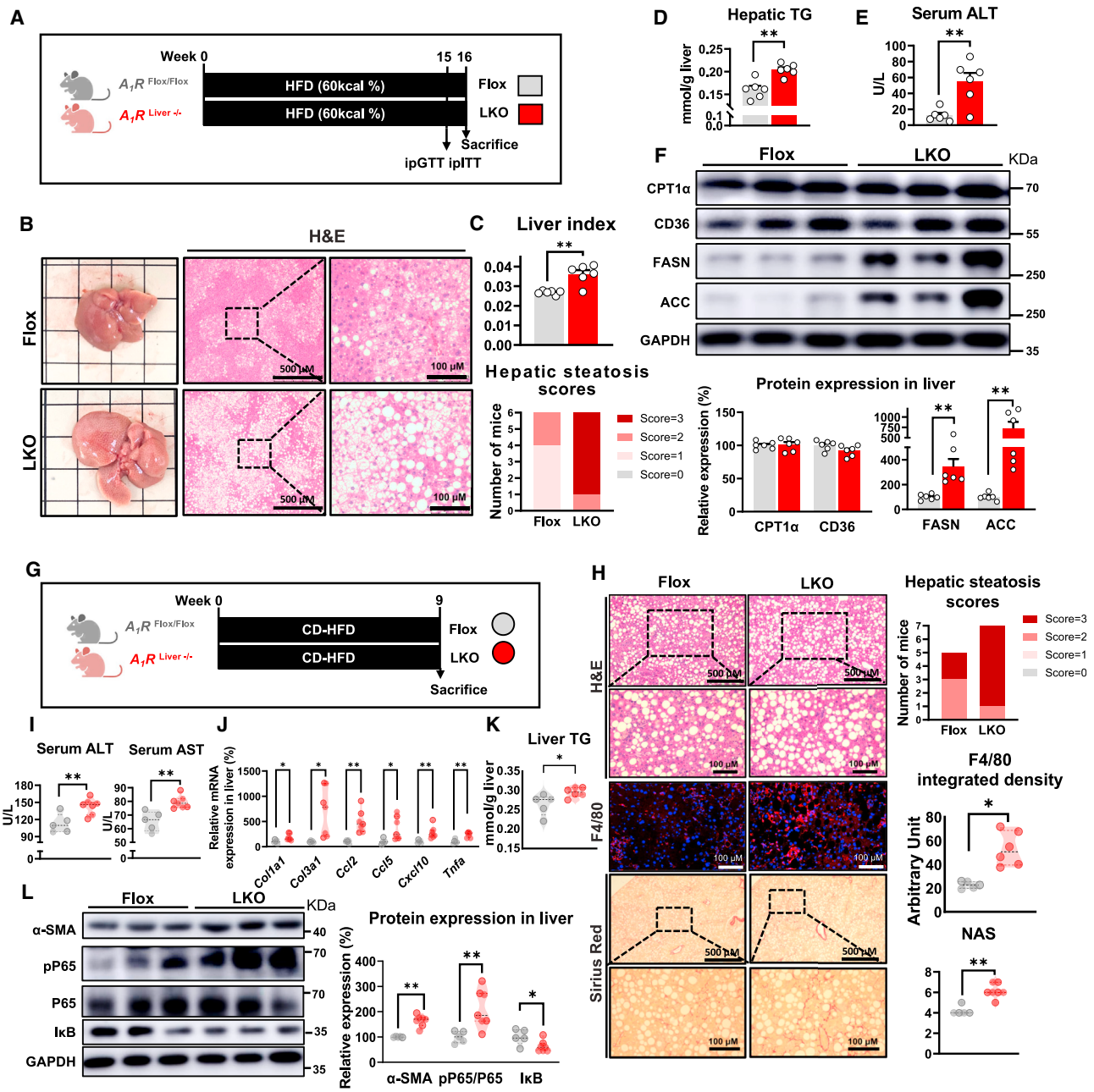

Figure 1. Liver-specific A_1R knockout exaggerates MAFL and MASH in mice

(A–F) Control mice ($A_1R^{Flox/Flox}$ without Cre, Flox) and liver-specific A_1R knockout mice ($A_1R^{Liver-/-}$, LKO) were fed an HFD (60 kcal%) for 16 weeks (n = 6). (A) Diagram of experimental design. (B) Representative image of liver and liver H&E staining. (C) Hepatic steatosis scores and liver index. (D) Quantification of hepatic triglycerides (TGs). (E) The level of serum alanine aminotransferase (ALT). (F) Relative protein expression of CPT1α, CD36, FASN, and ACC.

(G–K) Flox mice and LKO mice were fed a calorie-restricted HFD (CD-HFD) for 9 weeks (n = 5∼7). (G) Diagram of experimental design. (H) H&E, F4/80, and Sirius red staining of liver sections, with histological evaluation. (I) Liver injury indicators, including serum ALT and AST. (J) mRNA expression in liver. Results are normalized for *18S*. (K) Quantification of hepatic triglycerides (TGs).

(L) Relative protein expression of α-SMA, pP65, P65, and IκB. GAPDH functioned as a reference protein. Results are representative of one biological replicate. Data are depicted as mean ± SEM. Student's unpaired t test; *p < 0.05, **p < 0.01.

was also validated in LKO mice, in which the hepatic A_1R expression was rescued by AAVs-mediated A_1R overexpression (LKO^{Res}, Figure S2J). Rescue of hepatic A_1R protected mice from HFD-induced MAFL, including improved hepatic steatosis, and reduced hepatic TG accumulation and liver injury (Figures S2K–S2N). Beside the preventive effect, overexpression of hepatic A_1R also exerted a therapeutic effect on the established MAFL in HFD-fed mice (Figures S2O–S2R). Collectively, these

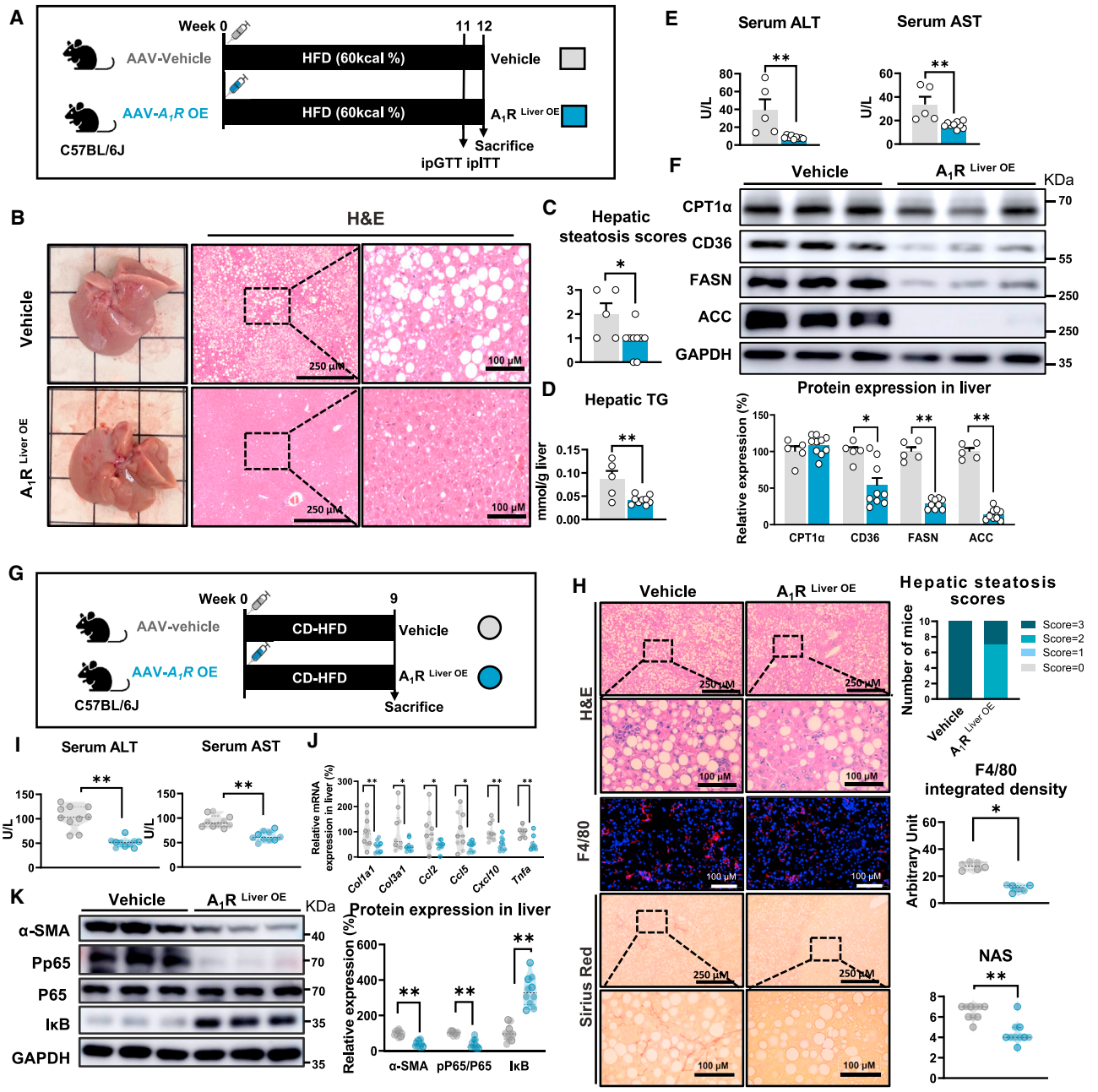

Figure 2. Liver-specific A_1R overexpression protects mice from MAFL and MASH in mice

(A–F) C57BL/6J mice were inoculated with vehicle-AAV (vehicle) or *A_1R*-overexpression-AAV ($A_1R^{Liver\ OE}$) intravenously, and then were fed an HFD for 12 weeks (n = 5∼9). (A) Diagram of experimental design. (B) Representative image of liver and liver H&E staining. (C) Hepatic steatosis scores. (D) Quantification of hepatic TG. (E) Liver injury indicators, including serum ALT and AST. (F) Relative protein expression of CPT1α, CD36, FASN, and ACC.

(G–K) Vehicle mice and $A_1R^{Liver\ OE}$ mice were fed a CD-HFD for 9 weeks (n = 10). (G) Diagram of experimental design. (H) H&E (n = 10), F4/80 (n = 6), and Sirius red staining (n = 10) of liver sections, with histological evaluation. (I) Liver injury indicators, including serum ALT and AST. (J) mRNA expression in liver. (K) Relative protein expression of α-SMA, pP65, P65, and IκB. Results are representative of one biological replicate. Data are depicted as mean ± SEM. Student's unpaired t test; *p < 0.05, **p < 0.01.

results indicated that hepatic A_1R activation attenuated diet-induced MAFL in mice.

We then tested whether overexpression of hepatic A_1R could also ameliorate MASH formation by feeding CD-HFD in mice. Our results showed that $A_1R^{Liver\ OE}$ mice had reduced lipid accumulation, fibrosis, and macrophage infiltration in liver, as well as reduced serum ALT and AST levels (Figures 2G–2I, S2S, and S2T). Furthermore, hepatic A_1R activation suppressed the

mRNA expression of fibrosis markers, chemotactic markers, and inflammatory cytokines, as well as the protein expression of α-SMA and pP65/P65, but it increased IκB expression (Figures 2J and 2K). In addition, the anti-MASH effect by activating hepatic A_1R was further confirmed in a 28-week AMLN diet-induced MASH mouse model,[37,38] as indicated by reduced hepatic steatosis, NAS, Sirius red staining, and improved liver function (Figures S2U–S2Z). Altogether, these results demonstrated activation of hepatic A_1R protected mice from diet-induced MAFL and MASH.

A_1R controls the maturation of SREBPs via PKAc

SREBPs (mainly SREBP1c and SREBP2) are critical nuclear transcriptional factors that regulating the DNL, cholesterol ,and inflammation signaling pathways in hepatocytes that are involved in MAFLD formation.[39] To investigate whether the hepatic A_1R regulates the MAFL and MASH development and progression through modulation on SREBPs, we measured the hepatic expression of precursor SREBPs (full-length SREBPs [flSREBPs]) in whole-cell and mature SREBPs (cleaved form of flSREBPs) in the nucleus (nSREBPs) in both LKO and $A_1R^{Liver\ OE}$ mice under HFD or CD-HFD feeding. LKO mice showed reduced flSREBP1c and flSREBP2 but increased nSREBP1c and nSREBP2 in the nucleus compared to Flox mice, while $A_1R^{Liver\ OE}$ mice showed the opposite trend in diet-induced MAFL or MASH mice (Figure 3A), implying A_1R negatively controlled the maturation of SREBPs in hepatocytes.

Activated A_1R modulates the intracellular signaling molecules through decreasing adenylate cyclase (AC) activity in cytomembrane,[9] resulting in suppression of activity of cAMP/PKAc in cytoplasm controlling the downstream targets, including SREBPs. The negative control of PKAc by hepatic A_1R was confirmed in both LKO and $A_1R^{Liver\ OE}$ mice as well as in AML-12 cells treated by 8-cyclopentyl-1,3-dipropylxanthine (DPCPX) and CPA, specific antagonist and agonist of A_1R, respectively[9] (Figures 3B and 3C). However, the exact modulation on SREBPs by PKAc remains unclear because both positive and negative regulation of SREBPs by cAMP/PKAc were previously reported.[40,41] Thus, the nuclear translocation of mature SREBP1c and SREBP2 was measured in AML-12 cells under the treatment of either DPCPX or CPA alone, or in combination with H89, a selective and potent inhibitor of PKA,[42] or dibutyryl-cAMP sodium salt (DbcAMP), a cell-permeable PKA activator by mimicking the action of endogenous cAMP.[43] The results showed the translocation of SREBP1c and SREBP2 to nucleus was stimulated by DPCPX but suppressed by CPA, whereas the combined treatment of H89 or DbcAMP reversed the SREBP nuclear translocation under DPCPX or CPA, as shown by consistent observations with either western blot or immunofluorescence. These results suggested the controlling of SREBP endonuclear content by A_1R was dependent on PKAc (Figures 3C–3E, S3A, and S3B).

To further evaluate the contribution of increased PKAc to MAFL formation in LKO mice, H89 was administered to either Flox or LKO mice during the 8 weeks of HFD feeding (Figure S3C). H89 treatment significantly improved hepatic steatosis and reduced ALT activity in both Flox and LKO mice (Figures S3D–S3I). In addition, the nuclear level of mature SREBP1c (nSREBP1c) was dramatically reduced by H89 in both Flox and LKO groups (Figure S3J). In summary, hepatic A_1R inhibited the nuclear translocation of SREBPs by decreasing PKAc, resulting in the attenuation of MAFLD.

A_1R reduces the cellular content of SCAP and its anchoring at Golgi membrane

The maturation of SREBPs is tightly controlled by SCAP and insulin-induced gene 1 protein (INSIG1) in endoplasmic reticulum (ER) escorting SREBPs from ER to Golgi apparatus where SREBPs is sequentially cleaved by two proteases: S1P and S2P[44,45] (Figure 4A). To explore how A_1R controlled the maturation of SREBPs, we tested the expression of these proteins in liver tissue of either LKO or $A_1R^{Liver\ OE}$ mice. We found only SCAP and S2P protein were significantly increased in LKO mice and decreased in $A_1R^{Liver\ OE}$ mice compared to their counterparts (Figures 4B; S4A).

Because the transport of SCAP from ER to Golgi apparatus and anchoring is the critical step for facilitating the maturation of SREBPs,[46] we then further explored the anchoring status of SCAP at Golgi apparatus by using 3D modeling of confocal image. As expected, inhibition of A_1R by DPCPX not only increased the cellular content of SCAP protein but also increased its anchoring at Golgi apparatus (yellow color in merged image and co-localization in 3D image), while CPA showed the opposite effect (Figure 4C), implying the negative regulation of SCAP content and function by A_1R. Given the established regulation of PKAc-SREBPs by the A_1R and SCAP-SREBPs axis,[46] we further asked whether the regulation of SCAP by A_1R was dependent on PKAc. The observations *in vitro* showed that the effects of CPA and DPCPX on SCAP protein content were abolished by co-treatment with H89 or DbcAMP, respectively (Figure 4D), suggesting A_1R might control the cellular content of SCAP protein through PKAc. Meanwhile, the binding between PKAc and SCAP was facilitated by DPCPX but suppressed by CPA (Figure S4B), implying A_1R inhibited the direct binding between PKAc and SCAP. Altogether, these results indicated that A_1R reduced intracellular SCAP content as well as its anchoring at Golgi membrane through PKAc.

A_1R activation accelerates SCAP protein degradation through SQSTM1 in lysosome

The cellular protein content is determined by the balance between synthesis and degradation. To test whether A_1R regulated the degradation of SCAP protein, AML-12 cells were treated with either CPA or DPCPX in the presence of cycloheximide (CHX), an inhibitor of protein biosynthesis. The results showed that CPA dramatically accelerated the degradation of SCAP, which was maintained stable by DPCPX in the presence of CHX treatment (Figure 5A), implying A_1R may control the cellular content of SCAP protein by accelerating its degradation. In line with the impact of PKAc on SCAP content, we found that the degradation of SCAP protein was accelerated by H89 but maintained by DbcAMP (Figure S4C), suggesting PKAc also controlled the degradation of SCAP. There are two major pathways regulating protein catabolism: the ubiquitin-proteasome system and the autophagy-lysosomal system.[47] To determine how A_1R controlled the SCAP

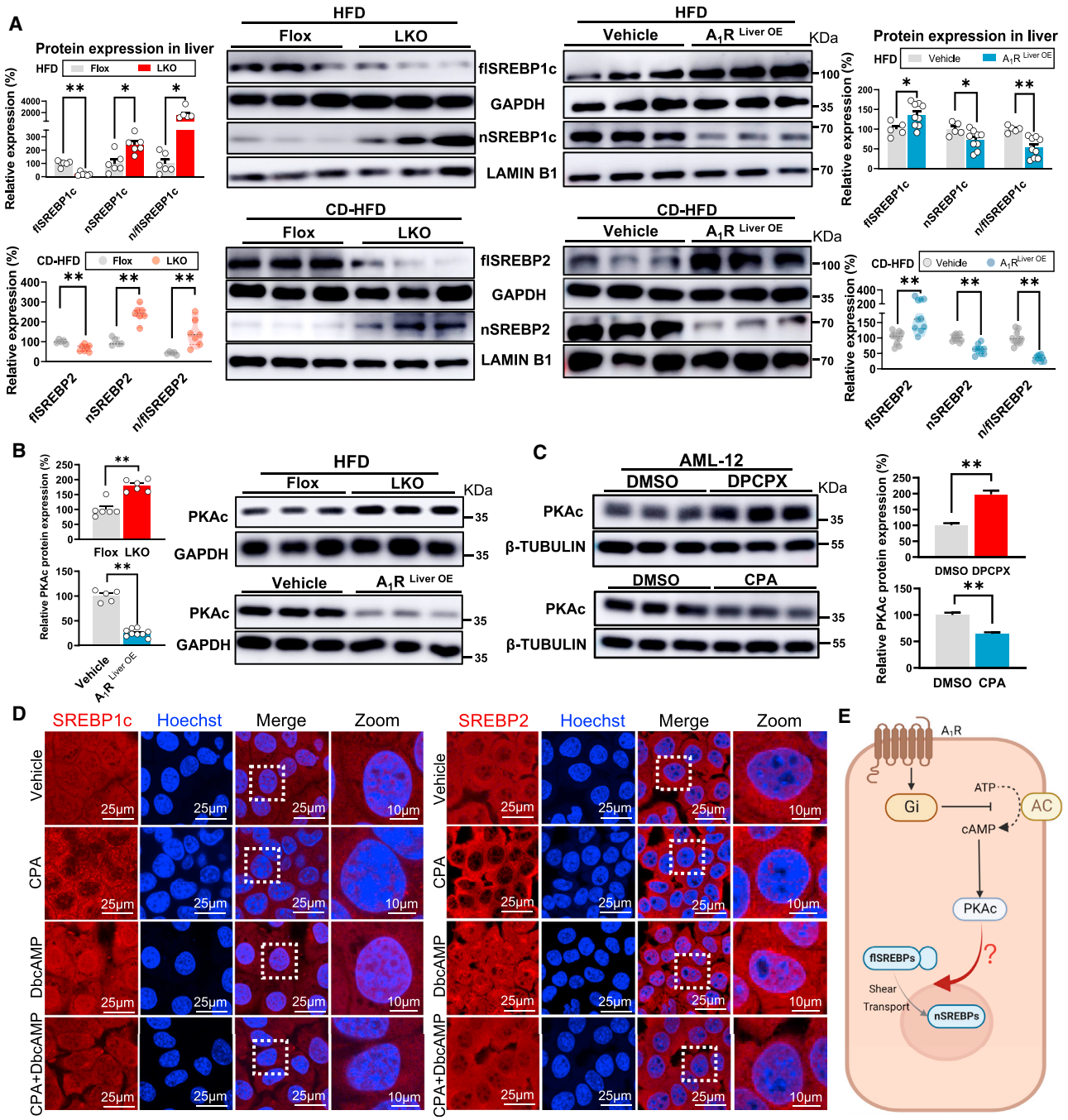

Figure 3. A_1R controls the maturation of SREBPs via PKAc

(A) Relative hepatic protein expression of flSREBP1c and nSREBP1c from LKO mice and $A_1R^{Liver\ OE}$ mice on HFD and CD-HFD.

(B) Hepatic PKAc protein expression in LKO and $A_1R^{Liver\ OE}$ mice.

(C) PKAc protein expression in AML-12 cells treated with CPA (A_1R activator, 1 μM) and DPCPX (A_1R inhibitor, 1 μM) for 48 h. GAPDH or tubulin was used as total protein control, and lamin B1 was used as nuclear protein control.

(D) AML-12 cells were treated with CPA (1 μM, 48 h), DbcAMP (PKA activator, 200 μM, 12 h), or co-treated with CPA and DbcAMP, respectively. Fluorescent staining of SREBP1c or SREBP2 (red) in each group was performed. The nuclei were stained by Hoechst (blue).

(E) Overview of A_1R intracellular signaling pathways. Activated A_1R decreases adenylate cyclase (AC) activity to suppress the activity of cAMP/PKAc in cytoplasm, resulting in modulation of the intracellular signaling molecules. However, the exact modulation on SREBPs by PKAc remains unclear. Image created using BioRender. Results are representative of one biological replicate. Data are depicted as mean ± SEM. Student's unpaired t test; *$p < 0.05$, **$p < 0.01$.

CellPress
OPEN ACCESS

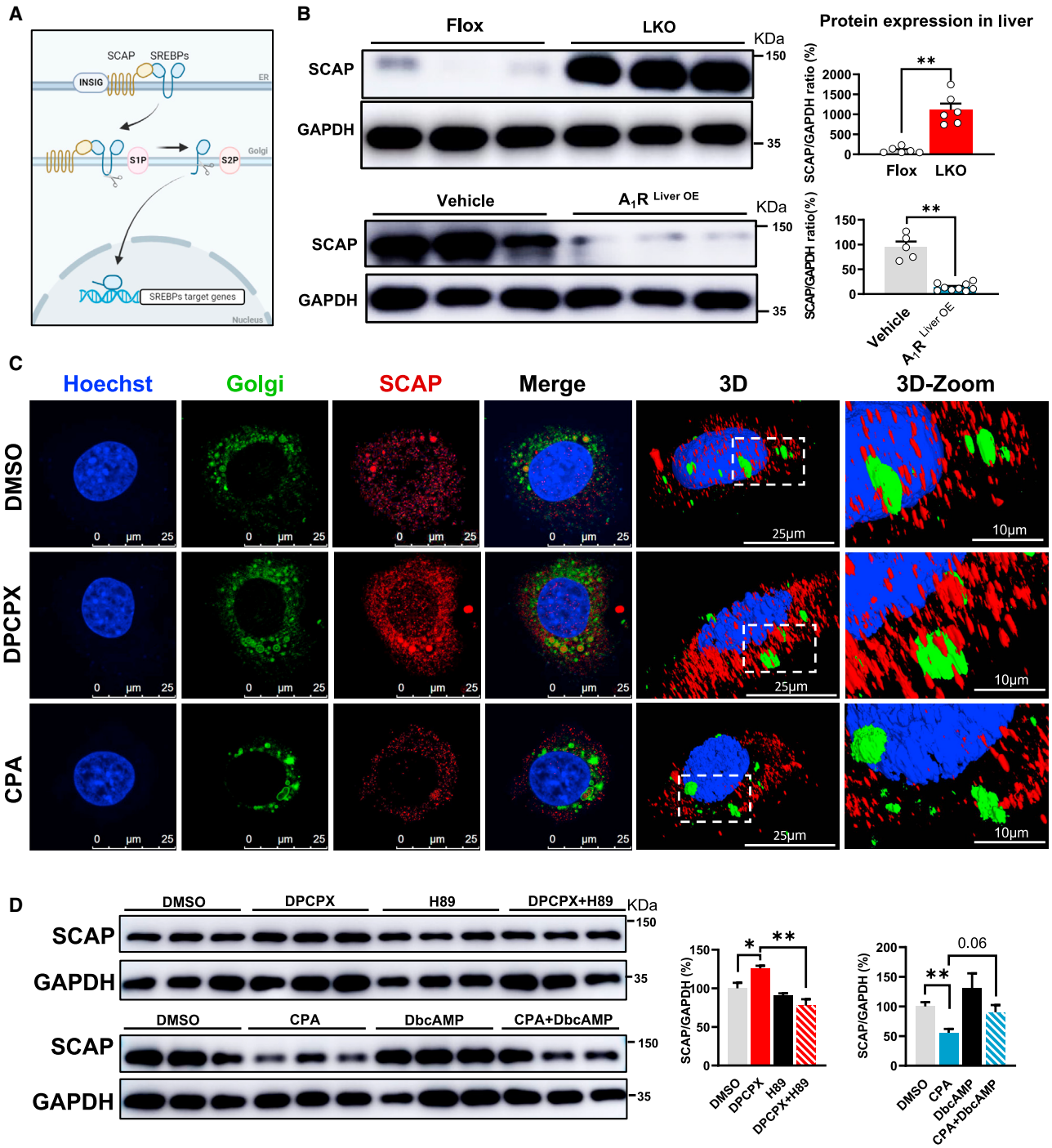

Figure 4. A_1R reduces the cellular content of SCAP and its anchoring at Golgi membrane

(A) Maturation process of SREBPs. SREBPs are exported from the ER to the Golgi apparatus by SCAP, and then transcriptional activation domain of SREBPs is released from the membrane by S1P and S2P. The released domain migrates into the nucleus and activates their transcription. Image created using BioRender.

(B) Protein expression of SCAP in the liver of $A_1R^{Liver\ OE}$ or LKO mice.

(C) SCAP colocalizes with the Golgi apparatus. AML-12 cells were treated with DPCPX (1 μM) or CPA (1 μM) for 48 h. Fluorescent staining of nuclei (Hoechst, blue), Golgi (green), and SCAP (red) in each group was performed.

(D) Protein expression of SCAP in the AML-12 cells treated or co-treated with CPA and DbcAMP (200 μM, 12 h), or DPCPX and H89 (20 μM, 4 h). Results are representative of one biological replicate. Cell experiments performed n = 3. Data are depicted as mean ± SEM. Student's unpaired t test; *p < 0.05, **p < 0.01.

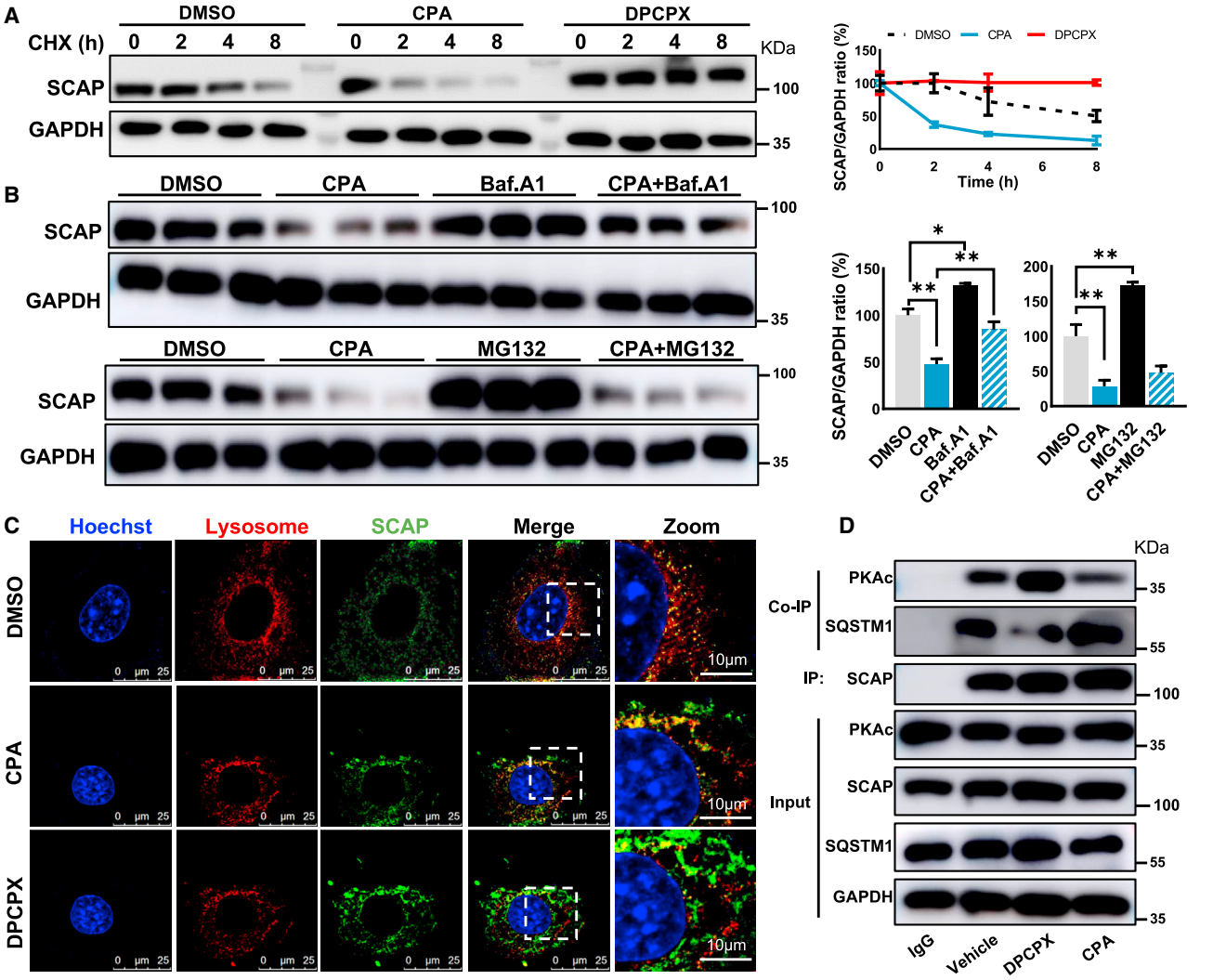

(legend on next page)

degradation, bafilomycin A1 (Baf.A1), blocking autophagosome-lysosome fusion and inhibiting protein degradation in lysosomes, or MG132, a potent proteasome and calpain inhibitor,[48] was co-treated with CPA in AML-12 cells, respectively. Results showed that coculture of Baf.A1, but not MG132, with CPA prevented the accelerated SCAP degradation induced by CPA (Figure 5B), suggesting that CPA may mainly accelerate SCAP degradation in lysosome. Further evidence was consistently observed by immunofluorescence, in which CPA increased the co-localization of SCAP with lysosome (yellow color in merged image), but not in DPCPX-treated cells (Figure 5C). These results indicated activated A_1R promoted the degradation of SCAP in lysosome.

We next investigated how A_1R controlled SCAP degradation. Recently, Zheng et al. revealed that SCAP was captured by SQSTM1 after it exited from ER and underwent a novel SQSTM1-mediated autophagy-independent lysosomal degradation.[48] Given the role of PKAc in maintaining cellular content of SCAP (Figures 4D and S4C) and the physical binding with SCAP directly (Figure S4B), we hypothesized that the increased degradation of SCAP by activated A_1R was due to the competitive binding with SCAP between PKAc and SQSTM1. The co-immunoprecipitation (Co-IP) test showed that CPA stimulated the formation of SCAP-SQSTM1 and reduced SCAP-PKAc complex, whereas the opposite effect was observed in DPCPX-treated cells (Figure 5D). Moreover, in agreement with the coIP observation, proximity ligation assay (PLA) revealed that CPA reduced the direct interaction between PKAc and SCAP but increased SQSTM1 and SCAP interaction, which was oppositely regulated by DPCPX (Figures 5E and 5F). Therefore, the results indicated that activated A_1R promoted the competitive binding of SCAP with SQSTM1 rather than PKAc, leading to SCAP degradation in lysosome.

Pharmacological hepatic A_1R activation attenuates MAFL and MASH in mice

Since the exact status of hepatic A_1R in MAFLD remains unclear, we examined the expression of A_1R protein in liver specimens from clinical patients. A total of 30 liver samples from a group of patients who underwent hepatectomy were retrospectively studied with immunohistology, in which 22 of them were diagnosed with the presence of hepatic steatosis, and eight of them were used as control without hepatic steatosis. The patient information is described in the supplementary methods (Table S1). The results showed universal positive expression of A_1R protein in hepatocytes in patients with hepatic steatosis but not in control patients (Figures 6A–6C). To further characterize the status of hepatic A_1R in MASH patients, the expression of hepatic A_1R was evaluated by using immunofluorescence in specimens from nine patients with MASH and four controls who underwent liver biopsy (Table S2). In agreement with the observation in patients with hepatic steatosis retrospectively, hepatic A_1R expression was obviously triggered in patients diagnosed with MASH but not in controls (Figures 6D–6F). Consistently, public clinical data also revealed the increased mRNA expression of *A_1R* in liver of patients with MAFLD[49,50] (Figure S4D, GSE89632, GSE135251). In agreement with these clinical findings, elevated hepatic A_1R protein expression was also present in HFD-fed mice time dependently or CD-HFD-fed mice compared to their chow diet controls (Figures S4E and S4F). As a result, we hypothesized that the elevated expression of hepatic A_1R in MAFLD patients or diet-induced MAFLD mice might be an adaptively protective response against MAFLD, but it is not sufficient.

To determine whether activation of A_1R signaling could protect against MAFLD, specific A_1R agonist CCPA (intraperitoneal [i.p.], 1 mg/kg once per day) was administered in both HFD-induced MAFL and CD-HFD-induced MASH mice (Figures S5A and S5L). The results showed CCPA treatment substantially improved the diet-induced MAFL and MASH in mice, including attenuation in hepatic steatosis and fibrosis in histology, and improvement in dyslipidemia, glucose intolerance (fasting blood glucose, insulin, and IGTT), liver function (serum ALT, AST, or alkaline phosphatase [ALP]), and inflammation (levels of serum IL-1β, IL-6 and TNF-α, and gene expression of chemokines), without affecting energy intake (Figures S5B–S5J and S5M–S5O). Moreover, CCPA treatment also suppressed the expression of FASN, ACC, PKAc, and SCAP protein; reduced maturation of SREBP1c/2 in MAFL mice; inhibited α-SMA; and enhanced IκB proteins in MASH mice (Figures S5K and S5Q). Collectively, these results demonstrated that pharmacological activation of hepatic A_1R was effective for MAFL and MASH therapy. To further test whether adenosine administration could also attenuate MAFLD in mice, we treated HFD-induced MAFLD mice with either adenosine (10 mg/kg, i.p.) or CCPA (1 mg/kg, i.p.) in parallel. As shown in Figures S6A–S6F, we found that even high doses of adenosine did not attenuate the extent of MAFLD, while specific A_1R agonist, CCPA, was effective in reducing lipid accumulation in hepatocytes and serum ALT/AST levels. These results suggested that the anti-MAFLD effect was due to specific activation of A1R but not in non-specific ligand of ARs.

Hepatic A_1R is an applicable target for screening MAFLD therapy compounds

Based on our current observations, we further asked whether hepatic A_1R was applicable for screening potential MAFLD

Figure 5. A_1R activation accelerates SCAP protein degradation through SQSTM1 in lysosome

(A) Relative protein expression of SCAP in the AML-12 cells treated with CPA or DPCPX in the presence of cycloheximide (CHX, 50 μM) for 0, 2, 4, and 8 h.

(B) Relative protein expression of SCAP in the AML-12 cells treated or co-treated with CPA and bafilomycin A1 (Baf.A1, lysosomal inhibitor, 1 μM, 8 h) or MG132 (proteasome inhibitor, 10 μM, 8 h).

(C) SCAP colocalizes with the lysosome. AML-12 cells were treated with DPCPX or CPA for 48 h. Fluorescent staining of nuclei (Hoechst, blue), lysosome (red), and SCAP (green) was performed.

(D) Co-immunoprecipitation (coIP) of PKAc or SQSTM1 with SCAP in the AML-12 cells treated with DPCPX or CPA for 12 h.

(E and F) Representative results and quantification of the proximity ligation assay (PLA) analysis of (E) PKAc or (F) SQSTM1 with SCAP in the AML-12 cells treated with CPA or DPCPX. Results are representative of one biological replicate. Cell experiments performed n = 3. Data are depicted as mean ± SEM. Student's unpaired t test; *$p < 0.05$, **$p < 0.01$.

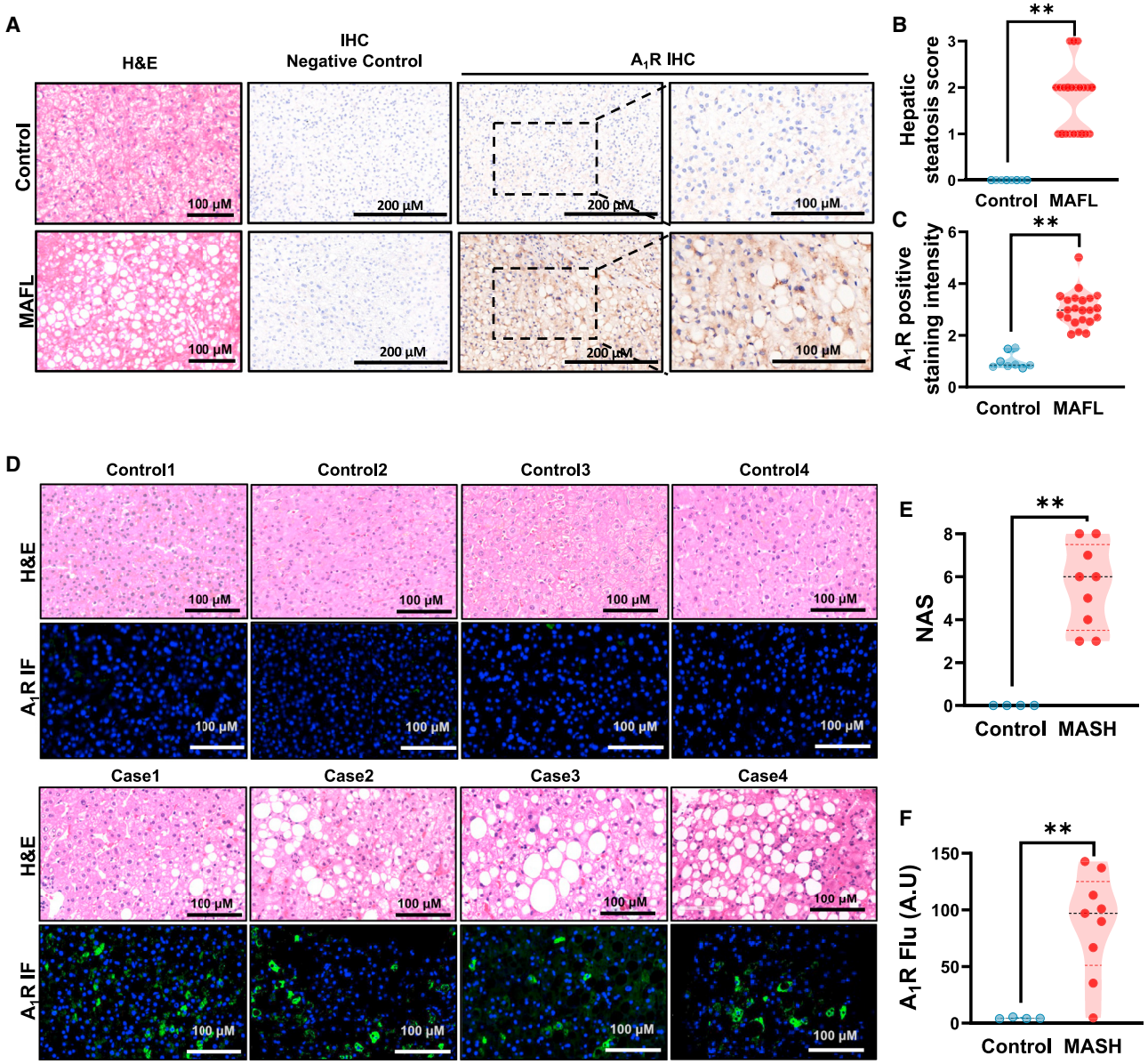

Figure 6. Hepatic A_1R negatively correlates with the advance of MAFLD

(A) Representative images showing H&E staining and A_1R immunohistochemical (IHC) staining of liver tissue from individuals with or without hepatic steatosis (n = 8∼22).

(B) Hepatic steatosis score.

(C) A_1R IHC-positive staining intensity.

(D) Representative images showing H&E staining and A_1R immunofluorescence staining of livers from healthy control or MASH individuals (n = 9).

(E) NAFLD activity score (NAS).

(F) A_1R fluorescence-positive staining intensity. Results are representative of one biological replicate. Data are depicted as mean ± SEM. Student's unpaired t test; *p < 0.05, **p < 0.01.

therapy compounds. For this purpose, we then screened natural compounds with activating capacity on A_1R among $3{,}600^{+}$ natural compounds library by using computer-aid molecular docking and followed by *in vitro* test on inhibition of cAMP production and TG accumulation. A total of 200 compounds stood out based on their binding free energy with A_1R, then 12 of them were selected with stronger activating capacity on A_1R than CCPA in A_1R-overexpressed HEK293T cells by measuring production of cAMP. At last, a natural component, timosaponin AIII (TA3), was identified based on its potent activating A_1R capacity, inhibition of intracellular TG production in primary hepatocytes from WT mice, and AML-12 and HepG2 cells dose dependently but not in primary hepatocytes from LKO mice (Figure 7A, S6G-J). TA3 also

CellPress
OPEN ACCESS

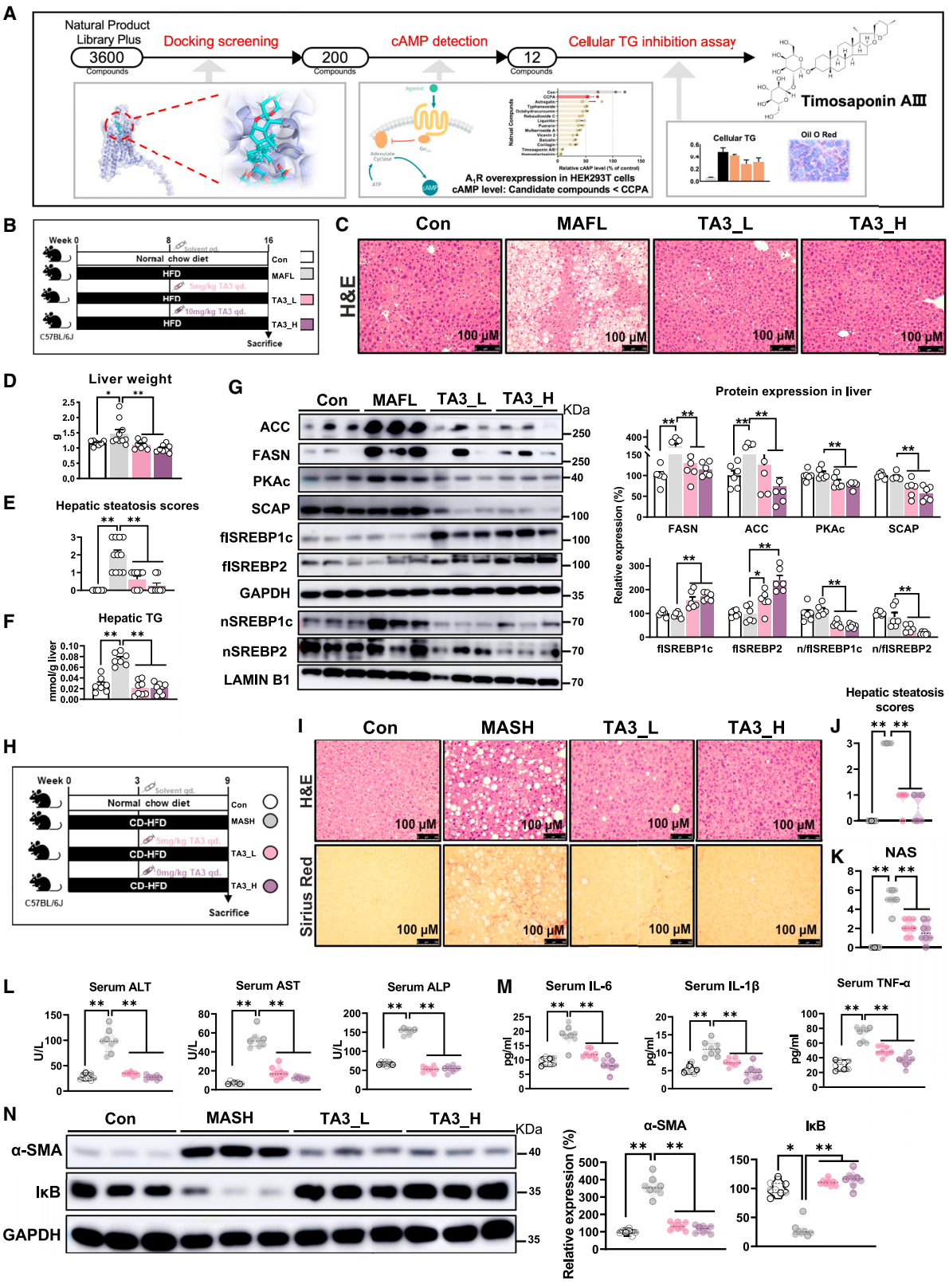

(legend on next page)

dose-dependently inhibited the expression of PKAc, FASN, ACC, and nuclear localization of nSREBP1c/2 in AML-12 cells, which were consistent with those of CCPA treatment or $A_1R^{Liver\ OE}$ mice (Figures S6K, S5K, 3A, and 3B). Additionally, ligand activation assay indicated that TA3 was strongest in reducing intracellular cAMP content in AML-12, HEK293T or A_1R-overexpressed HEK293T cells compared to CCPA or adenosine, endogenous ligand for ARs (Figure S6L). Moreover, we observed that adenosine had no effect on cAMP content, intracellular TG accumulation, or protein expression of ACC and FASN in AML-12 or HEK293T cells, while reduced cAMP content was only observed in A_1R-overexpressed HEK293T cells (Figures S6L–S6N), implying selectivity on A_1R was necessary for suppressing TG accumulation.

To evaluate the potential of TA3 as a novel MAFLD therapeutic candidate, the anti-MAFLD effect of TA3 was evaluated in HFD-induced MAFL and CD-HFD-induced MASH mice (5 or 10 mg/kg, i.p., once per day) (Figures 7B and 7H). As expected, TA3 treatment obviously attenuated HFD-induced MAFL, as shown by improved hepatic steatosis in histology, liver TG, and serum total cholesterol (TC), ALT, and AST (Figures 7C–7F and S7A–S7D). In line with the effects of CCPA (Figure S5K), TA3 suppressed the expression of PKAc, SCAP, ACC, and FASN as well as the maturation of SREBP1c/2, resulting in inhibition of DNL (Figure 7G). In parallel, TA3 treatment also effectively ameliorated CD-HFD-induced MASH, as shown by reduced hepatic steatosis, liver injury, and fibrosis based on histology; reduced serum inflammation cytokines; as well as related gene and protein expressions (Figures 7I–7N, S7E, and S7F). Taken together, these results indicated that the screened TA3 by targeting A_1R was effective for MAFL and MASH therapy, highlighting the potential of hepatic A_1R as MAFLD therapy target.

To further determine whether hepatic A_1R was the key therapeutic target for MAFLD, the anti-MASH effect of either CCPA (1 mg/kg, i.p., once per day) or TA3 (10 mg/kg, i.p., once per day) was tested in LKO mice that were fed with CD-HFD and treated with an identical dosage to that in WT mice (Figure S7G). To our expectation, both CCPA and TA3 treatment did not improve the histological change or the scores of hepatic steatosis and NAS, and they had minor impacts on serum parameters in LKO mice (Figures S7G–S7J), in contrast to their significant effects in WT mice (Figures 7 and S5). Consistently, neither CCPA nor TA3 reversed the expression of serum inflammation cytokines or hepatic α-SMA and IκB in CD-HFD-fed LKO mice (Figures S7K and S7L).

Altogether, these results revealed a novel role of hepatic A_1R as an anti-MAFLD therapeutic target, especially for MASH therapy.

DISCUSSION

We report here that hepatic A_1R activation protected mice from diet-induced MAFL and MASH. Activated hepatic A_1R reduced the cellular content of SCAP protein and its anchoring at Golgi apparatus due to increased lysosomal degradation by forming SCAP-SQSTM1 complex rather than SCAP-PKAc. The reduced cellular SCAP resulted in less formation of mature SREBP1c/2 and nuclear SREBP1c/2 translocation, leading to reduced DNL and inflammation. The anti-MAFLD role of hepatic A_1R was further confirmed by specific A_1R agonist CCPA and screened natural compound TA3 with potent activating capacity on A_1R activity, which implied that the observed increase of A_1R expression in liver of MAFL/MASH patients or MAFLD mice might be an adaptive response against MAFLD development and progression.

The four subtypes of ARs are widely distributed with diversified functions and involved in various pathophysiological processes upon activation by extracellular adenosine.[9] Extracellular adenosine can be released from intracellular stores, and is predominantly derived from the metabolism of precursor nucleotides ATP/ADP by CD39 and CD73 catalyzation, especially in pathological conditions such as inflammation and hypoxia.[11,51] The adenosine signaling could be terminated by adenosine uptake from the extracellular compartment into cytoplasm through equilibrative nucleoside transporter 1 (ENT1) and equilibrative nucleoside transporter 2 (ENT2) where adenosine is converted to AMP through adenosine kinase or to inosine through the adenosine deaminase.[52–54] A_1R is mainly expressed in central nervous system and some peripheral organs where extracellular adenosine performs different functions in a cell-type-dependent way.[9,55,56] Blocking A_1R-mediated signaling could abolish heart-rate-slowing effects of intravascular adenosine. Since the four subtypes of ARs are present in hepatocytes, or partly expressed in stellate cells, Kupffer cells, and sinusoidal endothelial cells,[9,57] previous study suggested that the number and affinity of A_1R and A_3R did not change in cirrhotic and fatty livers but the numbers of $A_{2A}R$ and $A_{2B}R$ increase in cirrhotic and fatty livers.[31] In agreement with the observation that disrupted $A_{2A}R$ exacerbated MAFLD development in $A_{2A}R$-deficient mice,[58] our findings showed a higher ratio of hepatocytes with positive A_1R

Figure 7. Timosaponin AIII, an identified potent A_1R activator, inhibits diet-induced MAFL and MASH in mice

(A) Schematic of the drug screen.

(B–G) C57BL/6J mice were fed with HFD for 16 weeks and injected intraperitoneally with 0.9% NaCl solution (MAFL) or 5 or 10 mg/kg timosaponin AIII (TA3) daily from ninth week (n = 7–~10). (B) Diagram of experimental design. (C) Representative image of liver H&E staining. (D) Liver weight. (E) Hepatic steatosis scores. (F) Quantification of hepatic TG. (G) Relative protein expression of PKAc, SCAP, SREBPs (flSREBP1c, flSREBP2, nSREBP1c, nSREBP2), and SREBP1c regulated proteins (FASN, ACC) (n = 6).

(H–N) C57BL/6J mice were fed a normal chow diet (NCD, Con) or CD-HFD for 9 weeks; during the process, CD-HFD mice were divided into three subgroups and injected intraperitoneally with 0.9% NaCl solution (CD-HFD) or 5 or 10 mg/kg TA3 daily from fourth week. (H) Diagram of experimental design.

(I–N) C57BL/6J mice were fed with CD-HFD for 9 weeks and injected intraperitoneally with 0.9% NaCl solution (MASH) or 5 or 10 mg/kg timosaponin AIII (TA3) daily from fourth week (n = 8). (I) H&E and Sirius red staining of liver sections. (J and K) Histological evaluation. (L) Serum ALT, AST, and ALP. (M) Serum inflammatory cytokines. (N) Relative protein expression of α-SMA and IκB. GAPDH was used as total protein control; lamin B1 was used as nuclear protein control. Results are representative of one biological replicate. Data are depicted as mean ± SEM. One-way ANOVA analysis; *p < 0.05, **p < 0.01.

protein expression in liver of patients with MAFL/MASH or MAFLD mice than their healthy controls. In addition, we observed the expression of these four ARs in mouse liver, in which A1R was the highest among them in both male and female (Figure S4G). We therefore questioned whether the increased adenosine and hepatic A_1R signaling contributed to the development of MAFLD or was an adaptive response for combating MAFLD development instead. To answer this question, genetic deletion of hepatic A_1R in LKO mice served as an ideal model, rather than global A_1R knockout mice, which makes it hard to exclude the impacts derived from A_1R deletion in other organs. To our surprise, LKO mice were more prone to diet-induced MAFL and MASH than Flox mice, which was also reversely validated in $A_1R^{Liver\ OE}$ mice, and, moreover, rescue of hepatic A_1R attenuated hepatic steatosis in LKO mice. In contrast to the report by Peng et al. that global knockout of either A_1R or $A_{2B}R$ protected mice against ethanol-induced fatty liver disease,[31] our results demonstrated that hepatic A_1R activation would attenuate diet-induced MAFL/MASH based on liver-specific A_1R knockout or overexpression mice. Meanwhile, the other three subtypes of ARs in liver of mice were not altered by the deletion or overexpression of hepatic A_1R. Therefore, our current findings revealed a previously unreported function of hepatic A_1R against MAFLD development, implying that increased expression of A_1R in liver in MAFLD patients or mice might be an adaptive response instead of causative for MAFLD development.

Sterol-regulatory element binding proteins (mainly SREBP1c and SREBP2) are essential transcription factors activating the expression of genes in DNL and cholesterol synthesis[59,60] and promoting inflammation, and they are crucial for MAFL and MASH formation.[61] In agreement with the phenotypes in LKO or $A_1R^{Liver\ OE}$ mice, the maturation and nuclear translocation process of SREBPs was stimulated by A_1R deletion and inhibited by A_1R overexpression, as well as consistent observation by A_1R antagonist DPCPX or agonist CPA *in vitro*. The premature SREBPs are synthesized as ER membrane-bound proteins that are activated upon sterol through the escorting from ER to Golgi apparatus by SCAP.[46,61,62] Consistent with the changes of nSREBPs upon A_1R activation or inhibition either *in vivo* or *in vitro*, cellular content of SCAP protein was increased by A_1R deletion and decreased by A_1R activation, as well as its anchoring at Golgi apparatus. Previous studies showed liver-specific deletion of SCAP caused low SREBPs protein and mRNA expression, resulting in marked reduction of both the precursor and nSREBPs.[63–65] In contrast, our results suggested that activated A_1R blocked the maturation and translocation to nucleus of SREBPs by reducing cellular SCAP content, instead of the suppression of SREBP generation because of the observed accumulation of flSREBPs in cytoplasm. This discrepancy between ours and a previous report might be due to the altered cellular SCAP content controlled by A_1R in our model, which was different from the direct impact on SREBPs by liver-specific *Scap* knockout.

There are several other signal pathways that are tightly controlled by A_1R, including cAMP/PKA, PLCβ-IP3-PKC, and MAPK family such as ERK, p38, and JNK.[66,67] Nevertheless, the role of cAMP/PKA in A_1R-controlled TG accumulation was also validated by intervention of A_1R agonist CCPA in the presence or absence of PKA agonist or inhibitors of PKC, ERK, p38, and JNK *in vitro*. These results showed that only PKA agonist abolished the inhibitory effect of cellular TG accumulation upon A_1R activation, while inhibitors of PKC, ERK, p38, and JNK did not (data not shown). So, it was concluded that cAMP/PKA might mediate the subsequent intracellular signal upon A_1R activation. cAMP/PKA is known to coordinate with the SCAP-SREBPs pathway through controlling SCAP phosphorylation.[68] In our study, although we observed that specific PKA inhibitor, H89, attenuated hepatic steatosis and nSREBP1c content in liver of LKO mice, our phosphoproteomic analyses of PKA-dependent phosphorylated targets excluded the possibility of SCAP phosphorylation in response to A_1R suppression (Figure S4H) but facilitated the co-localization of SCAP protein in lysosome instead. PKA is a heterotetrametric holoenzyme in which two catalytic subunits from two major families, Cα/β, combine with homodimers formed by any of four R-subunits (RIα, RIβ, RIIα, RIIβ) to form a number of R2:C2 holoenzymes.[69–72] Canonically, PKA is activated when cAMP binds to the regulatory subunits, triggering release of the catalytic subunit PKAc.[73] We observed that the catalytic subunit PKAc was reduced upon A_1R activation or increased by A_1R inhibition, which was consistently accompanied by SCAP-SREBP alteration. Since we did not observe the evidence of SCAP phosphorylation by PKA upon A_1R activity inhibition, we then postulated that the SCAP content might be modulated by A_1R through direct binding with PKAc, which was shown by the following coIP test.

The cellular content of protein is tightly controlled by the balance between biosynthesis and degradation. We demonstrated that activation of A_1R by CPA increased the degradation of SCAP protein in the context of inhibiting protein biosynthesis with CHX. Moreover, CPA increased SCAP co-localization and degradation in lysosome, instead of the ubiquitin-proteasome system, which are the two major pathways regulating protein catabolism.[47] In agreement with our current finding, Zheng et al. revealed an autophagy-independent SCAP degradation in lysosome through binding with SQSTM1 induced by the small molecule lycorine.[48] It is unclear whether A_1R controlled the lysosomal SCAP degradation via SQSTM1. We observed that A_1R activation resulted in increased binding of SCAP with SQSTM1 or promoted the formation of SCAP-PKAc complex upon A_1R inhibition, as shown by both co-IP and PLA tests. These results implicated an interestingly competitive binding of SCAP with SQSTM1 rather than PKAc upon A_1R activation, facilitating SCAP degradation in lysosome and then reducing maturation of SREBPs. This is a new mechanism underlying the process of A_1R controlling the PKAc-SCAP-SREBPs pathway.

Finally, in agreement with the protection of hepatic A_1R against MAFLD development based on liver-specific knockout or overexpression of A_1R mice, pharmacological activation of A_1R by specific agonist CCPA, a lead compound for improving lung function, ischemia reperfusion, neuro-protection, and anticonvulsant activity,[74–77] also effectively attenuated diet-induced MAFL and MASH in mice. Moreover, the potential of A_1R as an anti-MAFLD target was validated by the screened natural compound TA3 based on its potent ability for A_1R activation. TA3 is a well-established lead compound with multiple-pharmacological activities, including

anti-cancer, anti-neuronal disorders, anti-inflammation, and anti-coagulant,[78] while our results demonstrated its anti-MAFLD effect by activating A_1R. Notably, both CCPA and TA3 were effective in treating diet-induced MAFL and MASH in WT mice, but not in LKO mice, implicating that hepatic A_1R is the target of pharmacological agonists for MAFLD therapy instead of other tissues.

In summary, our current study reveals a previously undetermined role of hepatic A_1R as anti-MAFLD drug target and elucidates the underlying mechanism by controlling the PKAc-SCAP-SREBPs pathway. The increased expression of hepatic A_1R in MAFLD patients might be an adaptive response to combating MAFLD development, but it is not sufficient. Pharmacological activation of hepatic A_1R is practical for MAFLD treatment, in particular MASH.

Limitations of the study

In the current study, we demonstrated that genetic or pharmacological activation of hepatic A_1R inhibited MAFL/MASH development. The underlying mechanism was that activated A_1R promoted the competitive binding of SCAP with SQSTM1 rather than PKAc, leading to SCAP degradation in lysosome, which reduced SREBP maturation and its regulated DNL and inflammation. It should be noted that the main limitations of the study were summarized follows.

First, although our results demonstrated the control by A_1R on SCAP degradation through PKAc, the mechanistic insight into how A_1R regulates the competitive binding between PKAc and SQSTM1 with SCAP remains unclear; for example, the key binding site of SCAP with PKAc or SQSTM1 needs to be fully characterized.

Second, A_1R agonists of CCPA and TA3 were effective in treating MAFL/MASH; however, CCPA inhibited locomotor activity in mice but TA3 did not. Because both CCPA and TA3 could be detected in brain, we postulated that these two agonists might activate the A_1R in different ways, such as different binding structural domains of A_1R. Currently, the binding characteristics of these two agonists on A_1R were under in-depth exploration in cooperation with experts in the structural biology group. We believe the elucidation of the binding characteristics by agonists of CCPA or TA3 would accelerate the research and development of anti-MASH drugs by targeting activation of A_1R with more safety and fewer side effect in inhibition of central nervous system.

Third, although our results demonstrated that liver-specific deletion A_1R exacerbated the severity of MAFL/MASH, which was relieved by its liver-specific overexpression *in vivo* and *in vitro*, we could not completely rule out whether the observed effects might be partly attributed to the endogenous adenosine action on other subtypes of ARs, which are also implicated in metabolic diseases such as MAFLD.[58]

Fourth, the underlying mechanism of the elevated expression of hepatic A_1R both in MAFLD/MASH patients and mouse model was not addressed in our current report. Further investigation is warranted to uncover the exact mechanism that regulates the expression of hepatic A_1R during the development of MAFLD/MASH.

Finally, Stagg et al. recently demonstrated that $A_{2A}R$ protected against MASH-HCC development,[12] so it would be of interest to explore whether A_1R is also involved in the development of MASH-HCC in the future. Since TA3 has been reported to have anti-tumor effects on various tumor cells, including HCC,[79] we speculated that hepatic A_1R may be involved in the development of MASH-HCC. It should be noted that the presence and correlation of hepatic A_1R with pathological stages of MASH was only evaluated on nine liver specimens from MASH patients with liver biopsy in our current study. Further study is urgently needed by including a clinical cohort with large-scale MASH patients, which is of vital significance to translate current findings to the clinic.

STAR★METHODS

Detailed methods are provided in the online version of this paper and include the following:

- KEY RESOURCES TABLE
- RESOURCE AVAILABILITY
  - Lead contact
  - Materials availability
  - Data and code availability
- EXPERIMENTAL MODEL AND STUDY PARTIPANT DETAILS
  - Human samples and approval
  - Mice study and approval
  - HFD/CD-HFD diet feeding, AAV8 injection, and pharmacological treatment
- METHOD DETAILS
  - Generation of genetically modified mice
  - Cell lines
  - Serum insulin level test and HOMA-IR
  - Serum biochemistry index test
  - Inflammatory cytokines test
  - Liver triglycerides examination
  - Tissues staining
  - Histopathological evaluation
  - Liver F4/80 and CD11b immunofluorescence staining
  - Quantification of ^{13}C incorporated fatty acids
  - Oil red O staining for cells
  - Immunohistochemical staining and quantification
  - Immunofluorescence
  - Co-immunoprecipitation (Co-IP)
  - Proximity ligation assay (PLA)
  - Natural compound database screening
  - Protein isolation and western blot analyses
  - Extraction of total RNA and real-time quantitative PCR
- QUANTIFICATION AND STATISTICAL ANALYSIS
  - Data representation and statistical analysis

SUPPLEMENTAL INFORMATION

Supplemental information can be found online at https://doi.org/10.1016/j.xcrm.2024.101477.

ACKNOWLEDGMENTS

We sincerely acknowledge Prof. Jiayi Wang at Shanghai Chest Hospital for his generous contribution of the PLA probe kit (DUO92008), which helped us finish Figures 5E and 5F on time. We also acknowledge Prof. Gonghong Wei at

Fudan University for his help in analyzing the GWAS summary of MAFLD/MASH. This work was supported by the National Natural Science Foundation of China (nos. 81873059, 82374129 to H.L.), the Joint Funds of National Natural Science Foundation of China (no. U21A20413 to H.L.), Shanghai Excellent Academic Leaders Program (no. 21XD1403500 to H.L.), and Youth Qi Huang Scholar by State Administration of TCM (to H.L.).

AUTHOR CONTRIBUTIONS

W.Z. and Y.H. performed all experiments, data analysis, and figure arrangement and took part in manuscript writing. Z.T., X.Z., X.W., and Z.T. were responsible for clinical sample and patient information collection. P.S. was responsible for pathological diagnosis of MAFLD patients. X.H., Y.L., H.W., X.G., W.H., Z.L., Y.B., J.M., and N.Z. were involved in most of the animal experiments and data analysis. C.X. guided the mechanistic study and helped in the manuscript writing. X.K. guided the PLA experiment and data analysis. W.Z. assisted in screening and identification of TA3 compound from dozens of candidates. W.J. helped in the study design. J.Z. coordinated the clinical study of the project, including sample and patient information collection and A_1R analysis of clinical samples. L.S. took part in the study design, data analysis, and manuscript writing. M.L. participated in manuscript revision and data analysis. H.L. organized the studies, supervised the project, and revised the manuscript.

DECLARATION OF INTERESTS

The authors declare no competing interests.

Received: June 26, 2023
Revised: December 10, 2023
Accepted: February 21, 2024
Published: March 19, 2024

REFERENCES

1. Méndez-Sánchez, N., Bugianesi, E., Gish, R.G., Lammert, F., Tilg, H., Nguyen, M.H., Sarin, S.K., Fabrellas, N., Zelber-Sagi, S., Fan, J.G., et al. (2022). Global multi-stakeholder endorsement of the MAFLD definition. Lancet. Gastroenterol. Hepatol. *7*, 388–390. https://doi.org/10.1016/S2468-1253(22)00062-0.
2. Eslam, M., Newsome, P.N., Sarin, S.K., Anstee, Q.M., Targher, G., Romero-Gomez, M., Zelber-Sagi, S., Wai-Sun Wong, V., Dufour, J.F., Schattenberg, J.M., et al. (2020). A new definition for metabolic dysfunction-associated fatty liver disease: An international expert consensus statement. J. Hepatol. *73*, 202–209. https://doi.org/10.1016/j.jhep.2020.03.039.
3. Zhang, X.L., Fan, J.G., Wei, L., Shi, J.P., and Zheng, M.H.; Chinese MAFLD Clinical Research Network (2022). Promoting the term MAFLD: China in action. Lancet. Gastroenterol. Hepatol. *7*, 598. https://doi.org/10.1016/S2468-1253(22)00127-3.
4. Shiha, G., Korenjak, M., Eskridge, W., Casanovas, T., Velez-Moller, P., Högström, S., Richardson, B., Munoz, C., Sigurðardóttir, S., Coulibaly, A., et al. (2021). Redefining fatty liver disease: an international patient perspective. Lancet. Gastroenterol. Hepatol. *6*, 73–79. https://doi.org/10.1016/S2468-1253(20)30294-6.
5. Powell, E.E., Wong, V.W.S., and Rinella, M. (2021). Non-alcoholic fatty liver disease. Lancet *397*, 2212–2224. https://doi.org/10.1016/S0140-6736(20)32511-3.
6. Eslam, M., Sanyal, A.J., and George, J.; International Consensus Panel (2020). MAFLD: A Consensus-Driven Proposed Nomenclature for Metabolic Associated Fatty Liver Disease. Gastroenterology *158*, 1999–2014.e1. https://doi.org/10.1053/j.gastro.2019.11.312.
7. James, O.F., and Day, C.P. (1998). Non-alcoholic steatohepatitis (NASH): a disease of emerging identity and importance. J. Hepatol. *29*, 495–501. https://doi.org/10.1016/s0168-8278(98)80073-1.
8. Sawada, K., Chung, H., Softic, S., Moreno-Fernandez, M.E., and Divanovic, S. (2023). The bidirectional immune crosstalk in metabolic dysfunction-associated steatotic liver disease. Cell Metabol. *35*, 1852–1871. https://doi.org/10.1016/j.cmet.2023.10.009.
9. Borea, P.A., Gessi, S., Merighi, S., Vincenzi, F., and Varani, K. (2018). Pharmacology of Adenosine Receptors: The State of the Art. Physiol. Rev. *98*, 1591–1625. https://doi.org/10.1152/physrev.00049.2017.
10. Jain, S., and Jacobson, K.A. (2021). Purinergic Signaling in Liver Pathophysiology. Front. Endocrinol. *12*, 718429. https://doi.org/10.3389/fendo.2021.718429.
11. Le, T.T.T., Berg, N.K., Harting, M.T., Li, X., Eltzschig, H.K., and Yuan, X. (2019). Purinergic Signaling in Pulmonary Inflammation. Front. Immunol. *10*, 1633. https://doi.org/10.3389/fimmu.2019.01633.
12. Allard, B., Jacoberger-Foissac, C., Cousineau, I., Bareche, Y., Buisseret, L., Chrobak, P., Allard, D., Pommey, S., Ah-Pine, F., Duquenne, S., et al. (2023). Adenosine A2A receptor is a tumor suppressor of NASH-associated hepatocellular carcinoma. Cell Rep. Med. *4*, 101188. https://doi.org/10.1016/j.xcrm.2023.101188.
13. Slaats, J., Wagena, E., Smits, D., Berends, A.A., Peters, E., Bakker, G.J., van Erp, M., Weigelin, B., Adema, G.J., and Friedl, P. (2022). Adenosine A2a Receptor Antagonism Restores Additive Cytotoxicity by Cytotoxic T Cells in Metabolically Perturbed Tumors. Cancer Immunol. Res. *10*, 1462–1474. https://doi.org/10.1158/2326-6066.CIR-22-0113.
14. Giuffrida, L., Sek, K., Henderson, M.A., Lai, J., Chen, A.X.Y., Meyran, D., Todd, K.L., Petley, E.V., Mardiana, S., Mølck, C., et al. (2021). CRISPR/Cas9 mediated deletion of the adenosine A2A receptor enhances CAR T cell efficacy. Nat. Commun. *12*, 3236. https://doi.org/10.1038/s41467-021-23331-5 (2021.
15. Ehrentraut, H., Westrich, J.A., Eltzschig, H.K., and Clambey, E.T. (2012). Adora2b adenosine receptor engagement enhances regulatory T cell abundance during endotoxin-induced pulmonary inflammation. PLoS One *7*, e32416. https://doi.org/10.1371/journal.pone.0032416.
16. Ehrentraut, H., Clambey, E.T., McNamee, E.N., Brodsky, K.S., Ehrentraut, S.F., Poth, J.M., Riegel, A.K., Westrich, J.A., Colgan, S.P., and Eltzschig, H.K. (2013). CD73+ regulatory T cells contribute to adenosine-mediated resolution of acute lung injury. Faseb. J. *27*, 2207–2219. https://doi.org/10.1096/fj.12-225201.
17. Fishman, P., and Bar-Yehuda, S. (2003). Pharmacology and therapeutic applications of A3 receptor subtype. Curr. Top. Med. Chem. *3*, 463–469. https://doi.org/10.2174/1568026033392147.
18. Durante, M., Squillace, S., Lauro, F., Giancotti, L.A., Coppi, E., Cherchi, F., Di Cesare Mannelli, L., Ghelardini, C., Kolar, G., Wahlman, C., et al. (2021). Adenosine A3 agonists reverse neuropathic pain via T cell-mediated production of IL-10. J. Clin. Invest. *131*, e139299. https://doi.org/10.1172/JCI139299.
19. Koeppen, M., Eckle, T., and Eltzschig, H.K. (2009). Selective deletion of the A1 adenosine receptor abolishes heart-rate slowing effects of intravascular adenosine in vivo. PLoS One *4*, e6784. https://doi.org/10.1371/journal.pone.0006784.
20. Jakova, E., Moutaoufik, M.T., Lee, J.S., Babu, M., and Cayabyab, F.S. (2022). Adenosine A1 receptor ligands bind to alpha-synuclein: implications for alpha-synuclein misfolding and alpha-synucleinopathy in Parkinson's disease. Transl. Neurodegener. *11*, 9. https://doi.org/10.1186/s40035-022-00284-3.
21. Badimon, A., Strasburger, H.J., Ayata, P., Chen, X., Nair, A., Ikegami, A., Hwang, P., Chan, A.T., Graves, S.M., Uweru, J.O., et al. (2020). Negative feedback control of neuronal activity by microglia. Nature *586*, 417–423. https://doi.org/10.1038/s41586-020-2777-8 (2020.
22. Peleli, M., and Carlstrom, M. (2017). Adenosine signaling in diabetes mellitus and associated cardiovascular and renal complications. Mol. Aspect. Med. *55*, 62–74. https://doi.org/10.1016/j.mam.2016.12.001.

23. Dhalla, A.K., Chisholm, J.W., Reaven, G.M., and Belardinelli, L. (2009). A1 adenosine receptor: role in diabetes and obesity. Handb. Exp. Pharmacol., 271–295. https://doi.org/10.1007/978-3-540-89615-9_9.

24. Laties, A., Rich, C.C., Stoltz, R., Humbert, V., Brickman, C., McVicar, W., and Baumgartner, R.A. (2016). A Randomized Phase 1 Dose Escalation Study to Evaluate Safety, Tolerability, and Pharmacokinetics of Trabodenoson in Healthy Adult Volunteers. J. Ocul. Pharmacol. Therapeut. *32*, 548–554. https://doi.org/10.1089/jop.2015.0147.

25. Lu, L.J., Tsai, J.C., and Liu, J. (2017). J. Novel Pharmacologic Candidates for Treatment of Primary Open-Angle Glaucoma. Yale J. Biol. Med. *90*, 111–118.

26. Thursz, M.R., Richardson, P., Allison, M., Austin, A., Bowers, M., Day, C.P., Downs, N., Gleeson, D., MacGilchrist, A., Grant, A., et al. (2015). Prednisolone or pentoxifylline for alcoholic hepatitis. N. Engl. J. Med. *372*, 1619–1628. https://doi.org/10.1056/NEJMoa1412278.

27. Yang, M., Chu, R., Chisholm, J.W., Doege, H., Belardinelli, L., and Dhalla, A.K. (2012). Adenosine A(1) receptors do not play a major role in the regulation of lipogenic gene expression in hepatocytes. Eur. J. Pharmacol. *683*, 332–339. https://doi.org/10.1016/j.ejphar.2012.03.012.

28. Yang, P., Han, Z., Chen, P., Zhu, L., Wang, S., Hua, Z., and Zhang, J. (2010). A contradictory role of A1 adenosine receptor in carbon tetrachloride- and bile duct ligation-induced liver fibrosis in mice. J. Pharmacol. Exp. Therapeut. *332*, 747–754. https://doi.org/10.1124/jpet.109.162727.

29. Kim, J., Kim, M., Song, J.H., and Lee, H.T. (2008). Endogenous A1 adenosine receptors protect against hepatic ischemia reperfusion injury in mice. Liver Transplant. *14*, 845–854. https://doi.org/10.1002/lt.21432.

30. Yang, P., Chen, P., Wang, T., Zhan, Y., Zhou, M., Xia, L., Cheng, R., Guo, Y., Zhu, L., and Zhang, J. (2013). Loss of A1 Adenosine Receptor Attenuates Alpha-naphthylisothiocyanate-Induced Cholestatic Liver Injury in Mice. Toxicol. Sci. *131*, 128–138. https://doi.org/10.1093/toxsci/kfs263.

31. Peng, Z., Borea, P.A., Varani, K., Wilder, T., Yee, H., Chiriboga, L., Blackburn, M.R., Azzena, G., Resta, G., and Cronstein, B.N. (2009). Adenosine signaling contributes to ethanol-induced fatty liver in mice. J. Clin. Invest. *119*, 582–594. https://doi.org/10.1172/JCI37409.

32. Ramkumar, V., Stiles, G.L., Beaven, M.A., and Ali, H. (1993). The A3 adenosine receptor is the unique adenosine receptor which facilitates release of allergic mediators in mast cells. J. Biol. Chem. *268*, 16887–16890.

33. Matsumoto, M., Hada, N., Sakamaki, Y., Uno, A., Shiga, T., Tanaka, C., Ito, T., Katsume, A., and Sudoh, M. (2013). An improved mouse model that rapidly develops fibrosis in non-alcoholic steatohepatitis. Int. J. Exp. Pathol. *94*, 93–103. https://doi.org/10.1111/iep.12008.

34. Gao, X.M., Dong, W.H., Xia, C.L., Ma, Z.Y., Wang, Y., Sarra, S., Xu, H.M., and Qi, W.Y. (2022). Centranthera grandiflore alleviates alcohol-induced oxidative stress and cell apoptosis. Chin. J. Nat. Med. *20*, 572–579. https://doi.org/10.1016/S1875-5364(22)60181-X.

35. Zhou, S., Fan, K.K., Gu, L.F., Yu, B.Y., and Chai, C.Z. (2022). Anti-inflammatory effects of Abelmoschus manihot (L.) Medik. on LPS-induced cystitis in mice: potential candidate for cystitis treatment based on classic use. Chin. J. Nat. Med. *20*, 321–331. https://doi.org/10.1016/S1875-5364(22)60140-7.

36. Zhang, X., Sharma, P., Maschmeyer, P., Hu, Y., Lou, M., Kim, J., Fujii, H., Unutmaz, D., Schwabe, R.F., and Winau, F. (2023). GARP on hepatic stellate cells is essential for the development of liver fibrosis. J. Hepatol. *79*, 1214–1225. https://doi.org/10.1016/j.jhep.2023.05.043.

37. Zhao, P., Sun, X., Chaggan, C., Liao, Z., In Wong, K., He, F., Singh, S., Loomba, R., Karin, M., Witztum, J.L., and Saltiel, A.R. (2020). An AMPK-caspase-6 axis controls liver damage in nonalcoholic steatohepatitis. Science *367*, 652–660. https://doi.org/10.1126/science.aay0542.

38. Clapper, J.R., Hendricks, M.D., Gu, G., Wittmer, C., Dolman, C.S., Herich, J., Athanacio, J., Villescaz, C., Ghosh, S.S., Heilig, J.S., et al. (2013). Diet-induced mouse model of fatty liver disease and nonalcoholic steatohepatitis reflecting clinical disease progression and methods of assessment. Am. J. Physiol. Gastrointest. Liver Physiol. *305*, G483–G495. https://doi.org/10.1152/ajpgi.00079.2013.

39. Horton, J.D., Goldstein, J.L., and Brown, M.S. (2002). SREBPs: activators of the complete program of cholesterol and fatty acid synthesis in the liver. J. Clin. Invest. *109*, 1125–1131. https://doi.org/10.1172/JCI15593.

40. Lee, J.H., Lee, G.Y., Jang, H., Choe, S.S., Koo, S.H., and Kim, J.B. (2014). Ring finger protein20 regulates hepatic lipid metabolism through protein kinase A-dependent sterol regulatory element binding protein1c degradation. Hepatology *60*, 844–857. https://doi.org/10.1002/hep.27011.

41. Yan, F., Wang, Q., Lu, M., Chen, W., Song, Y., Jing, F., Guan, Y., Wang, L., Lin, Y., Bo, T., et al. (2014). Thyrotropin increases hepatic triglyceride content through upregulation of SREBP-1c activity. J. Hepatol. *61*, 1358–1364. https://doi.org/10.1016/j.jhep.2014.06.037.

42. Chijiwa, T., Mishima, A., Hagiwara, M., Sano, M., Hayashi, K., Inoue, T., Naito, K., Toshioka, T., and Hidaka, H. (1990). Inhibition of forskolin-induced neurite outgrowth and protein phosphorylation by a newly synthesized selective inhibitor of cyclic AMP-dependent protein kinase, N-[2-(p-bromocinnamylamino)ethyl]-5-isoquinolinesulfonamide (H-89), of PC12D pheochromocytoma cells. J. Biol. Chem. *265*, 5267–5272.

43. Coqueret, O., Demarquay, D., and Lagente, V. (1996). Role of cyclic AMP in the modulation of IgE production by the beta 2-adrenoceptor agonist, fenoterol. Eur. Respir. J. *9*, 220–225. https://doi.org/10.1183/09031936.96.09020220.

44. Kim, J.Y., Garcia-Carbonell, R., Yamachika, S., Zhao, P., Dhar, D., Loomba, R., Kaufman, R.J., Saltiel, A.R., and Karin, M. (2018). ER Stress Drives Lipogenesis and Steatohepatitis via Caspase-2 Activation of S1P. Cell *175*, 133–145.e15. https://doi.org/10.1016/j.cell.2018.08.020.

45. Osborne, T.F., and Espenshade, P.J. (2009). Evolutionary conservation and adaptation in the mechanism that regulates SREBP action: what a long, strange tRIP it's been. Genes Dev. *23*, 2578–2591. https://doi.org/10.1101/gad.1854309.

46. Brown, M.S., Radhakrishnan, A., and Goldstein, J.L. (2018). Retrospective on Cholesterol Homeostasis: The Central Role of Scap. Annu. Rev. Biochem. *87*, 783–807. https://doi.org/10.1146/annurev-biochem-062917-011852.

47. Goldberg, A.L. (2013). Encyclopedia of Biological Chemistry, Second Edition, W.J. Lennarz and M. Daniel Lane, eds. (Academic Press), pp. 617–624.

48. Zheng, Z.G., Zhu, S.T., Cheng, H.M., Zhang, X., Cheng, G., Thu, P.M., Wang, S.P., Li, H.J., Ding, M., Qiang, L., et al. (2021). Discovery of a potent SCAP degrader that ameliorates HFD-induced obesity, hyperlipidemia and insulin resistance via an autophagy-independent lysosomal pathway. Autophagy *17*, 1592–1613. https://doi.org/10.1080/15548627.2020.1757955.

49. Arendt, B.M., Comelli, E.M., Ma, D.W.L., Lou, W., Teterina, A., Kim, T., Fung, S.K., Wong, D.K.H., McGilvray, I., Fischer, S.E., and Allard, J.P. (2015). Altered Hepatic Gene Expression in Nonalcoholic Fatty Liver Disease Is Associated With Lower Hepatic n-3 and n-6 Polyunsaturated Fatty Acids. Hepatology *61*, 1565–1578. https://doi.org/10.1002/hep.27695.

50. Govaere, O., Cockell, S., Tiniakos, D., Queen, R., Younes, R., Vacca, M., Alexander, L., Ravaioli, F., Palmer, J., Petta, S., et al. (2020). Transcriptomic profiling across the nonalcoholic fatty liver disease spectrum reveals gene signatures for steatohepatitis and fibrosis. Sci. Transl. Med. *12*, eaba4448. https://doi.org/10.1126/scitranslmed.aba4448.

51. Bowser, J.L., Lee, J.W., Yuan, X., and Eltzschig, H.K. (1985). The hypoxia-adenosine link during inflammation. J. Appl. Physiol. *123*, 1303–1320. https://doi.org/10.1152/japplphysiol.00101.2017.

52. Aherne, C.M., Collins, C.B., Rapp, C.R., Olli, K.E., Perrenoud, L., Jedlicka, P., Bowser, J.L., Mills, T.W., Karmouty-Quintana, H., Blackburn, M.R., and Eltzschig, H.K. (2018). Coordination of ENT2-dependent adenosine transport and signaling dampens mucosal inflammation. JCI Insight *3*, e121521. https://doi.org/10.1172/jci.insight.121521.

53. Eckle, T., Hughes, K., Ehrentraut, H., Brodsky, K.S., Rosenberger, P., Choi, D.S., Ravid, K., Weng, T., Xia, Y., Blackburn, M.R., and Eltzschig, H.K. (2013). Crosstalk between the equilibrative nucleoside transporter ENT2 and alveolar Adora2b adenosine receptors dampens acute lung injury. Faseb. J. *27*, 3078–3089. https://doi.org/10.1096/fj.13-228551.

54. Ruan, W., Li, J., Choi, S., Ma, X., Liang, Y., Nair, R., Yuan, X., Mills, T.W., and Eltzschig, H.K. (2023). Targeting myocardial equilibrative nucleoside transporter ENT1 provides cardioprotection by enhancing myeloid Adora2b signaling. JCI Insight *8*, e166011. https://doi.org/10.1172/jci.insight.166011.

55. Chen, J.F., Eltzschig, H.K., and Fredholm, B.B. (2013). Adenosine receptors as drug targets–what are the challenges? Nat. Rev. Drug Discov. *12*, 265–286. https://doi.org/10.1038/nrd3955.

56. Dunwiddie, T.V., and Masino, S.A. (2001). The role and regulation of adenosine in the central nervous system. Annu. Rev. Neurosci. *24*, 31–55. https://doi.org/10.1146/annurev.neuro.24.1.31.

57. Jacobson, K.A., and Gao, Z.G. (2006). Adenosine receptors as therapeutic targets. Nat. Rev. Drug Discov. *5*, 247–264. https://doi.org/10.1038/nrd1983.

58. Cai, Y., Li, H., Liu, M., Pei, Y., Zheng, J., Zhou, J., Luo, X., Huang, W., Ma, L., Yang, Q., et al. (2018). Disruption of adenosine 2A receptor exacerbates NAFLD through increasing inflammatory responses and SREBP1c activity. Hepatology *68*, 48–61. https://doi.org/10.1002/hep.29777.

59. Buyl, K., Vrints, M., Fernando, R., Desmae, T., Van Eeckhoutte, T., Jans, M., Van Der Schueren, J., Boeckmans, J., Rodrigues, R.M., De Boe, V., et al. (2023). Human skin stem cell-derived hepatic cells as in vitro drug discovery model for insulin-driven de novo lipogenesis. Eur. J. Pharmacol. *957*, 175989. https://doi.org/10.1016/j.ejphar.2023.175989.

60. Xia, Q., Lu, F., Chen, Y., Li, J., Huang, Z., Fang, K., Hu, M., Guo, Y., Dong, H., Xu, L., and Gong, J. (2024). 6-Gingerol regulates triglyceride and cholesterol biosynthesis to improve hepatic steatosis in MAFLD by activating the AMPK-SREBPs signaling pathway. Biomed. Pharmacother. *170*, 116060. https://doi.org/10.1016/j.biopha.2023.116060.

61. Shimano, H., and Sato, R. (2017). SREBP-regulated lipid metabolism: convergent physiology - divergent pathophysiology. Nat. Rev. Endocrinol. *13*, 710–730. https://doi.org/10.1038/nrendo.2017.91.

62. Lee, S.H., Lee, J.H., and Im, S.S. (2020). The cellular function of SCAP in metabolic signaling. Exp. Mol. Med. *52*, 724–729. https://doi.org/10.1038/s12276-020-0430-0.

63. Tlapak-Simmons, V.L., Baggenstoss, B.A., Clyne, T., and Weigel, P.H. (1999). Purification and lipid dependence of the recombinant hyaluronan synthases from Streptococcus pyogenes and Streptococcus equisimilis. J. Biol. Chem. *274*, 4239–4245. https://doi.org/10.1074/jbc.274.7.4239.

64. Moon, Y.A., Liang, G., Xie, X., Frank-Kamenetsky, M., Fitzgerald, K., Koteliansky, V., Brown, M.S., Goldstein, J.L., and Horton, J.D. (2012). The Scap/SREBP Pathway Is Essential for Developing Diabetic Fatty Liver and Carbohydrate-Induced Hypertriglyceridemia in Animals. Cell Metabol. *15*, 240–246. https://doi.org/10.1016/j.cmet.2011.12.017.

65. Kober, D.L., Xu, S., Li, S., Bajaj, B., Liang, G., Rosenbaum, D.M., and Radhakrishnan, A. (2020). Identification of a degradation signal at the carboxy terminus of SREBP2: A new role for this domain in cholesterol homeostasis. Proc. Natl. Acad. Sci. USA *117*, 28080–28091. https://doi.org/10.1073/pnas.2018578117.

66. Schulte, G., and Fredholm, B.B. (2000). Human adenosine A(1), A(2A), A(2B), and A(3) receptors expressed in Chinese hamster ovary cells all mediate the phosphorylation of extracellular-regulated kinase 1/2. Mol. Pharmacol. *58*, 477–482.

67. Schulte, G., and Fredholm, B.B. (2003). Signalling from adenosine receptors to mitogen-activated protein kinases. Cell. Signal. *15*, 813–827. https://doi.org/10.1016/s0898-6568(03)00058-5.

68. Shimizu-Albergine, M., Van Yserloo, B., Golkowski, M.G., Ong, S.E., Beavo, J.A., and Bornfeldt, K.E. (2016). SCAP/SREBP pathway is required for the full steroidogenic response to cyclic AMP. Proc. Natl. Acad. Sci. USA *113*, E5685–E5693. https://doi.org/10.1073/pnas.1611424113.

69. Kornev, A.P., Aoto, P.C., and Taylor, S.S. (2022). Calculation of centralities in protein kinase A. Proc. Natl. Acad. Sci. USA *119*, e2215420119. https://doi.org/10.1073/pnas.2215420119.

70. Yang, J., Ten Eyck, L.F., Xuong, N.H., and Taylor, S.S. (2004). Crystal structure of a cAMP-dependent protein kinase mutant at 1.26A: new insights into the catalytic mechanism. J. Mol. Biol. *336*, 473–487. https://doi.org/10.1016/j.jmb.2003.11.044.

71. Sastri, M., Barraclough, D.M., Carmichael, P.T., and Taylor, S.S. (2005). A-kinase-interacting protein localizes protein kinase A in the nucleus. Proc. Natl. Acad. Sci. USA *102*, 349–354. https://doi.org/10.1073/pnas.0408608102.

72. Bastidas, A.C., Deal, M.S., Steichen, J.M., Guo, Y., Wu, J., and Taylor, S.S. (2013). Phosphoryl Transfer by Protein Kinase A Is Captured in a Crystal Lattice. J. Am. Chem. Soc. *135*, 4788–4798. https://doi.org/10.1021/ja312237q.

73. Dell'Acqua, M.L., and Scott, J.D. (1997). Protein kinase A anchoring. J. Biol. Chem. *272*, 12881–12884. https://doi.org/10.1074/jbc.272.20.12881.

74. Cheng, P., Zuo, X., Ren, Y., Bai, S., Tang, W., Chen, X., Wang, G., Wang, H., Huang, W., and Xie, P. (2016). Adenosine A1-Receptors Modulate mTOR Signaling to Regulate White Matter Inflammatory Lesions Induced by Chronic Cerebral Hypoperfusion. Neurochem. Res. *41*, 3272–3277. https://doi.org/10.1007/s11064-016-2056-0.

75. Fernandez, L.G., Sharma, A.K., LaPar, D.J., Kron, I.L., and Laubach, V.E. (2013). Adenosine A1 receptor activation attenuates lung ischemia-reperfusion injury. J. Thorac. Cardiovasc. Surg. *145*, 1654–1659. https://doi.org/10.1016/j.jtcvs.2013.01.006.

76. Meads, K.L., Thomas, T.P., Langston, J.L., Myers, T.M., and Shih, T.M. (2021). Evaluation of adenosine A1 receptor agonists as neuroprotective countermeasures against Soman intoxication in rats. Toxicol. Appl. Pharmacol. *416*, 115466. https://doi.org/10.1016/j.taap.2021.115466.

77. Fabera, P., Parizkova, M., Uttl, L., Vondrakova, K., Kubova, H., Tsenov, G., and Mares, P. (2019). Adenosine A1 Receptor Agonist 2-chloro-N6-cyclopentyladenosine and Hippocampal Excitability During Brain Development in Rats. Front. Pharmacol. *10*, 656. https://doi.org/10.3389/fphar.2019.00656.

78. Lin, Y., Zhao, W.R., Shi, W.T., Zhang, J., Zhang, K.Y., Ding, Q., Chen, X.L., Tang, J.Y., and Zhou, Z.Y. (2020). Pharmacological Activity, Pharmacokinetics, and Toxicity of Timosaponin AIII, a Natural Product Isolated From Anemarrhena asphodeloides Bunge: A Review. Front. Pharmacol. *11*, 764. https://doi.org/10.3389/fphar.2020.00764.

79. Zhang, L., Zhang, S., Jiang, M., Lu, L., Ding, Y., Ma, N., Zhao, Y., Xuchen, S., and Zhang, N. (2021). Novel Timosaponin AIII-Based Multifunctional Liposomal Delivery System for Synergistic Therapy Against Hepatocellular Carcinoma Cancer. Int. J. Nanomed. *16*, 5531–5550. https://doi.org/10.2147/IJN.S313759.

80. Hu, M., Zhang, D., Xu, H., Zhang, Y., Shi, H., Huang, X., Wang, X., Wu, Y., and Qi, Z. (2021). Salidroside Activates the AMP-Activated Protein Kinase Pathway to Suppress Nonalcoholic Steatohepatitis in Mice. Hepatology *74*, 3056–3073. https://doi.org/10.1002/hep.32066.

81. Hong, Y., Sheng, L., Zhong, J., Tao, X., Zhu, W., Ma, J., Yan, J., Zhao, A., Zheng, X., Wu, G., et al. (2021). Desulfovibrio vulgaris, a potent acetic acid-producing bacterium, attenuates nonalcoholic fatty liver disease in mice. Gut Microb. *13*, 1–20. https://doi.org/10.1080/19490976.2021.1930874.

82. Mansuy-Aubert, V., Zhou, Q.L., Xie, X., Gong, Z., Huang, J.Y., Khan, A.R., Aubert, G., Candelaria, K., Thomas, S., Shin, D.J., et al. (2013). Imbalance between neutrophil elastase and its inhibitor alpha1-antitrypsin in obesity alters insulin sensitivity, inflammation, and energy expenditure. Cell Metabol. *17*, 534–548. https://doi.org/10.1016/j.cmet.2013.03.005.

83. Matthews, D.R., Hosker, J.P., Rudenski, A.S., Naylor, B.A., Treacher, D.F., and Turner, R.C. (1985). Homeostasis model assessment: insulin

resistance and beta-cell function from fasting plasma glucose and insulin concentrations in man. Diabetologia *28*, 412–419. https://doi.org/10.1007/BF00280883.

84. Folch, J., Lees, M., and Sloane Stanley, G.H. (1957). A simple method for the isolation and purification of total lipides from animal tissues. J. Biol. Chem. *226*, 497–509.

85. Kleiner, D.E., Brunt, E.M., Van Natta, M., Behling, C., Contos, M.J., Cummings, O.W., Ferrell, L.D., Liu, Y.C., Torbenson, M.S., Unalp-Arida, A., et al. (2005). Design and validation of a histological scoring system for nonalcoholic fatty liver disease. Hepatology *41*, 1313–1321. https://doi.org/10.1002/hep.20701.

86. Mehlem, A., Hagberg, C.E., Muhl, L., Eriksson, U., and Falkevall, A. (2013). Imaging of neutral lipids by oil red O for analyzing the metabolic status in health and disease. Nat. Protoc. *8*, 1149–1154. https://doi.org/10.1038/nprot.2013.055.

87. Guo, S., Chen, Y., Yang, Y., Zhang, X., Ma, L., Xue, X., Qiao, Y., and Wang, J. (2021). TRIB2 modulates proteasome function to reduce ubiquitin stability and protect liver cancer cells against oxidative stress. Cell Death Dis. *12*, 42. https://doi.org/10.1038/s41419-020-03299-8.

STAR★METHODS

KEY RESOURCES TABLE

REAGENT or RESOURCE	SOURCE	IDENTIFIER
Antibodies		
A_1R antibody	Abcam, UK	ab151523
A_1R antibody	Abcam, UK	ab82477, RRID: AB_2049141
SREBP1c antibody	Abcam, UK	ab28481, RRID: AB_778069
SREBP2 antibody	Abclonal, China	A13049, RRID, AB_2759897
FASN antibody	Cell signaling, USA	#3180, RRID: AB_2100796
ACC antibody	Cell signaling, USA	#3676, RRID: AB_2219397
CPT1 antibody	Proteintech, USA	ag7202
CD36 antibody	Abcam, UK	ab133625, RRID, AB_2716564
F4/80 antibody	Servicebio, China	GB113373, RRID, AB_2938980
CD11B antibody	Boster, China	BM3925, RRID: AB_2832991
TGF-β antibody	Abclonal, China	A2124, RRID: AB_2764143
Smad2 antibody	Affinity, China	AF6449, RRID: AB_2835272
pSmad2 antibody	Affinity, China	AF3449, RRID: AB_2834844
PKAc antibody	Cell signaling, USA	#4782, RRID: AB_2170170
SCAP antibody	Cell signaling, USA	#13102, RRID: AB_2798121
SCAP antibody	Abmart, China	TD13713
SCAP antibody	SantaCruz, USA	SC-13553, RRID: AB_628237
S2P antibody	Abcam, UK	ab140594
S2P antibody	Affinity, USA	DF13911
S1P antibody	Abcam, UK	ab140592, RRID: AB_2811283
Insig1 antibody	Abcam, UK	ab70784, RRID: AB_1269181
SQSTM1 antibody	Abcam, UK	ab109012, RRID: AB_2810880
NF-κB P65 antibody	Proteintech, USA	66535–1, RRID: AB_2881898
Phospho-NF-κB p65 antibody	Cell signaling, USA	#3033s, RRID: AB_331284
α-SMA antibody	Cell signaling, USA	#19245, RRID: AB_2734835
IκBα antibody	Cell signaling, USA	#4814s, RRID: AB_390781
LAMIN B1 antibody	Cell signaling, USA	#13435, RRID: AB_2737428
β-TUBULIN antibody	Cell signaling, USA	#2146, RRID: AB_2210545
GAPDH antibody	Proteintech, USA	60004-1, RRID: AB_2107436
ATP1A1 antibody	PTM Bio, China	PTM-6271
Bacterial and virus strains		
AAV8-TBG-A_1R	This paper	N/A
AAV8-TGB-GFP	This paper	N/A
Biological samples		
Human liver paraffin blocks	This paper	N/A
Mouse liver paraffin blocks	This paper	N/A
Chemicals, peptides, and recombinant proteins		
CCPA	Aladdin, China	C170001
DPCPX	Sigma, USA	C101
CPA	Sigma, USA	C8301
H89	Selleck, China	S1582
DbcAMP	Selleck, China	S7858
Cycloheximide	Selleck, China	S7418

(*Continued on next page*)

Continued

REAGENT or RESOURCE	SOURCE	IDENTIFIER
MG132	MCE, USA	HY-13259
Bafilomycin A1	MCE, USA	HY-100558
Timosaponin AIII	MCE, USA	HY-N0810
PMSF	Beyotime, China	ST506
Critical commercial assays		
IL-1β ELISA Kit	Mlbio, China	ml301814
IL-6 ELISA Kit	Mlbio, China	ml063159
TNFα ELISA Kit	Mlbio, China	ml002095
Insulin ELISA Kit	Mlbio, China	ml001983V
PKA kinase activity kit	Enzo Life Sciences, USA	ADI-EKS-390A
cAMP Gi Kit	Cisbio, France	62a.m.9PEB
Hoechst	Beyotime, China	P0133
LysoTracker red	Beyotime, China	C1046
Golgi Staining Kit	Abcam, UK	ab139483
Mouse genotyping kit	Vazyme, China	PD101-01
FastKing gDNA Dispelling RT SuperMix	TIANGEN, China	KR118
qPCR SYBR Green Master Mix	Vazyme, China	Q131
RIPA Lysis Buffer	Beyotime, China	P0013B
Nuclear and Cytoplasmic Protein Extraction Kit	Beyotime, China	P0028
Triglycerides Assay Kit	Njjcbio, China	A110-1-1
Total cholesterol assay kit	Njjcbio, China	A111-1-1
Alanine aminotransferase Assay Kit	Njjcbio, China	C009-2-1
Aspartate aminotransferase Assay Kit	Njjcbio, China	C010-2-1
Alkaline phosphatase assay kit	Njjcbio, China	A059-2-2
Low-density lipoprotein cholesterol assay kit	Njjcbio, China	A113-1-1
High-density lipoprotein cholesterol assay kit	Njjcbio, China	A112-1-1
Nonesterified Free fatty acids assay kit	Njjcbio, China	A042-2-1
Oil Red O Stain Kit	Njjcbio, China	D027-1-2
Duolink *In Situ* Wash Buffers, Fluorescence	Sigma, USA	DUO82049
Duolink *In Situ* Detection Reagents Red	Sigma, USA	DUO92008
Duolink *In Situ* PLA Probe Anti-Rabbit PLUS	Sigma, USA	DUO92002
Duolink *In Situ* PLA Probe Anti-Mouse MINUS	Sigma, USA	DUO92004
Immunoprecipitation Kit	Invitrogen, USA	10007D
Membrane and Cytosol Protein Extraction Kit	Beyotime, China	P0033
EZ-press RNA purification kit	EZBio, USA	B0004DP
DMEM	Meilunbio, China	MA0212
DMEM/F-12	Meilunbio, China	MA0214
Deposited data		
Human NAFLD expression profiling data	GEO portal	GSE89632
Human NAFLD transcriptomic data	GEO portal	GSE135251
Experimental models: Cell lines		
AML12 cells	ATCC	CRL-2254
HepG2 cells	ATCC	HB-8065
Experimental models: Organisms/strains		
C57BL/6 *Adora1*$^{liver-/-}$ mice	Shanghai Model Organisms Center Inc.	N/A
Hepatic ADORA1-OE C57BL/6 mice	This paper	N/A
C57BL/6 mice	Shanghai SLAC Laboratory Animal Co., Ltd	N/A

(*Continued on next page*)

Continued

REAGENT or RESOURCE	SOURCE	IDENTIFIER
Oligonucleotides		
Primes for mouse see Table S3	This paper	N/A
Software and algorithms		
Prism, version 10	GraphPad	https://www.graphpad.com/
LAS X, version 3.5.7	Leica	https://www.leica.com/

RESOURCE AVAILABILITY

Lead contact

Further information and requests for resources and reagents should be directed to and will be fulfilled by the lead contact, Houkai Li (hk_li@shutcm.edu.cn).

Materials availability

This study did not generate new unique regents.

Data and code availability

- This paper analyzes existing, publicly available data. These accession numbers for the datasets are listed in the key resources table. All data reported in this paper will be shared by the lead contact upon reasonable request.
- This paper does not report original code.
- Any additional information required to reanalyze the data reported in this paper is available from the lead contact upon request.

EXPERIMENTAL MODEL AND STUDY PARTIPANT DETAILS

Human samples and approval

The patients' paraffin sections for A_1R IHC staining were collected from Huzhou Central Hospital (Zhejiang, China). The study protocol was approved by Medical Ethics Committee of Huzhou Central Hospital (No.20190401-02). The human liver samples for A_1R immunofluorescence that patients with biopsy-proven metabolic (dysfunction)-associate steatohepatitis (MASH) were recruited from Huzhou Central Hospital. This study procedures were approved by Medical Ethics Committee of Huzhou Central Hospital (No.20201201-02). All tissue samples were collected in compliance with informed consent policy. Clinical information is summarized in Tables S1 and S2. Each specimen was evaluated by experienced pathologists without knowledge of the clinical findings. The NAS consists of liver steatosis (scale of 0–3), lobular inflammation (scale of 0–3), hepatocellular ballooning (scale of 0–2).

Mice study and approval

Male C57BL/6J mice were housed under a 12:12-h light/dark cycle at controlled temperature conditions in specific-pathogen-free (SPF) condition. All animals were purchased from the Shanghai Model Organisms Center Inc, Shanghai SLAC Laboratory Animal Co., Ltd, and bred at the experimental animal center, Shanghai University of Traditional Chinese Medicine. All experimental procedures were approved by the Institutional Animal Care and Use Committee of Shanghai University of Traditional Chinese Medicine. All experiments were conducted in strict accordance with the Guidelines for the Investigation of Pain in Conscious Animal Experiments in order to minimize animal suffering and improve animal welfare (Ethical Approval Number: PZSHUTCM220221003, PZSHUTCM201030006, PZSHUTCM190426007, PZSHUTCM2304190012, PZSHUTCM2304190013).

HFD/CD-HFD diet feeding, AAV8 injection, and pharmacological treatment

Diet intervention started at 6-week-old. For diet induced MAFLD, mice were fed with high fat diet (HFD, 60% kcal from fat; D12492; Research Diets, New Brunswick, NJ, USA) for 12 or 16 weeks. To establish the NASH model, mice were fed with CD-HFD diet (A06071302, Research Diets, New Brunswick, NJ, USA) for 9 weeks or AMLN diet (Research Diet, Cat. D09100301, consisting of 40% fat, 20% fructose and 2% cholesterol) for 28 weeks.[37]

Hepatic *A_1R* overexpression mice ($A_1R^{Liver\ OE}$) were conducted via AAV8 mediated *A_1R* overexpression purchased from Shandong Vigene, vehicle-injected mice (pAV-TBG-P2A-GFP, Vehicle) were used as controls.

For PKA inhibition *in vivo*, PKA inhibitor H89 (1 mg/kg body weight, in 0.9% NaCl solution) was intraperitoneally injected into Flox and LKO mice daily with HFD feeding.[41] For CCPA treatment *in vivo*, CCPA (1 mg/kg body weight, in 0.9% NaCl solution) was injected into mice daily from 9th week of the 16-week HFD feeding, or from 4th week of the 9-week CD-HFD feeding, or from 13th week of the 28-week AMLN diet feeding. For adenosine treatment *in vivo*, adenosine (10 mg/kg, ip) or CCPA (1 mg/kg, ip) were treated from 13th week to 18th. For timosaponin AIII (TA3) treatment *in vivo*, TA3 (5, 10 mg/kg body weight, in 0.9% NaCl solution) was injected into mice daily from 4th week of the 9-week CD-HFD feeding.

All mice were fasted 12 h before the collection of blood and tissues. Serum was distributed into several centrifuge tubes for further analysis after being centrifuged at 4000 rpm for 15 min at 4°C. Mice tissue samples were used instantly or snap-frozen in liquid nitrogen and stored at −80°C after collection and being weighted.

METHOD DETAILS

Generation of genetically modified mice

Hepatic *A_1R* knockout mice (*$A_1R^{liver\ -/-}$*, LKO) was generated using the CRISPR/Cas9 system and Cre-loxP-mediated recombination technology. First, two single guide RNAs (sgRNA1 and sgRNA2) were used to target a fragment of *A_1R* exon3. Cas9 mRNA and gRNA were obtained by *in vitro* transcription. The donor vector was constructed by In-Fusion cloning, which contained a 3.0kb 5 'homology arm, a 1.0kb flox region and a 3.0kb 3' homology arm. Microinjection of Cas9 mRNA, gRNA, and donor vector into zygotes of C57BL/6J mice. We selected one founder mouse and crossed it with a C57BL/6J mouse to generate *A_1R*-Flox mice. Finally, the *A_1R* LKO mice were generated by crossing albumin-Cre recombinase (Alb-Cre) transgenic mice with *$A_1R^{flox/flox}$* mice. Littermates Alb-Cre negative, *$A_1R^{flox/flox}$* mice (Flox) were used as controls. Mice were housed in barrier facility with free access to drinking water and fed standard chow diet.

To generate hepatic *A_1R* over expression mice (*$A_1R^{liver\ OE}$*), AAV8-TBG-*A_1R* adenoviruses were injected intravenously (mousetail) at 10^12 vg per mice, single injection. The gene ID number is 11539, and transcript is NM_001008533.3 from Mus musculus. And control mice were injected with AAV8-TBG-GFP adenoviruses (Vehicle).

Cell lines

HepG2 cells were purchased from the Chinese Academy of Science (Shanghai, China), and were cultured in DMEM medium (Gibco, USA) supplemented with 10% FBS (BI, Israel), 100 U/ml penicillin and 100 mg/mL streptomycin (Meilunbio, China). AML-12 cells were cultured in DMEM medium (Gibco, USA) supplemented with 10% FBS (BI, Israel), 100 U/ml penicillin and 100 mg/mL streptomycin (Gibco, USA), 1% Insulin-Transferrin-Selenium-Sodium pyruvate (ITS-A) (Gibco, USA), 40 ng/mg dexamethasone (Sigma, USA).

For the stable *A_1R* over expression cell lines, AAV8-A_1R was purchased from Vigene Biosciences (Shandong). *A_1R* was over expressed in AML-12 cell line using pAV-TBG-P2A-GFP, packaged in Adeno-associated virus. AAV infection was carried out in 6-well plates by mixing 10 μL virus supernatant plus 10 mL complete medium with a final concentration of 10^{11} vg/ml. Then, the selection via fluorescence-activated cell sorter was performed 48 h after infection, and then infected cells were further grown for about 2 weeks in the medium. Identification of over expression was carried out by RT-qPCR and western blotting.

Mice primary hepatocytes were isolated from 8 to 12-week-old Flox or LKO mice by using collagenase perfusion and gradient centrifugation, as previously described.[80] Briefly, the mice liver was perfused with reperfusion buffer (135 mmol/L NaCl, 5.3 mmol/L KCl, 28.2 mmol/L $NaHCO_3$, 0.12 mmol/L Na_2HPO_4, 0.56 mmol/L NaH_2PO_4, 0.5 mmol/L EGTA, 9.0 g/L glucose, and 0.06 g/L Phenol red, PH 7.4) and enzyme buffer (135 mmol/L NaCl, 5.3 mmol/L KCl, 28.2 mmol/L $NaHCO_3$, 0.12 mmol/L Na_2HPO_4, 0.56 mmol/L NaH_2PO_4, 0.5 mmol/L EGTA, 10 mmol/L HEPES, and 0.06 g/L phenol red, 200 mg/L collagenase D and 3.8 mmol/L $CaCl_2$, PH7.4). The isolated primary hepatocytes were cultured in DMEM medium (Gibco, USA) supplemented 10% FBS (BI, Israel). Cells were grown at 37°C in a 5% CO_2 and 95% air atmosphere.

In vitro, cells were treated or co-treated with DPCPX (1 μM) for 48 h, CPA (1 μM) for 48 h, H89 (20 μM) for 4 h, DbcAMP (200 μM) for 12 h, and TA3 (0.5–10 μM) for 48 h, respectively. For mechanistic insight, cells were treated with cycloheximide (CHX, 50 μM) for 0, 2, 4, 8 h, bafilomycin A1 (Baf.A1, 1 μM) for 8 h, or MG132 (10 μM) for 8 h, in the presence of drugs.[48]

Intraperitoneal glucose tolerance test (ipGTT) and insulin tolerance test (ipITT)

For ipGTT, mice were fasted for 15 h overnight with free access to water, and then were injected intraperitoneally with glucose solution (1 g/kg body weight).[81] Fasting glucose levels were first measured as time 0, then blood glucose was examined at 15th, 30th, 60th, 90th, and 120th min after glucose injection. ipITT was performed by intraperitoneal injection with human insulin (0.75 units/kg body weight, Novo Nordisk) without fasting.[82]

Serum insulin level test and HOMA-IR

Homeostatic model assessment of insulin resistance (HOMA-IR) was employed to measure the fasting insulin levels in serum samples using a mouse Insulin ELISA kit. The following equation was used to determine the homeostasis model assessment of insulin resistance (HOMA-IR): HOMA-IR=(fasting glucose × fasting insulin)/22.5.[83]

Serum biochemistry index test

Serum cholesterol (TC), high-density lipoprotein cholesterol (HDL-C), low-density lipoprotein cholesterol (LDL-C), triglyceride (TG), alanine aminotransferase (ALT), aspartate aminotransferase (AST), and alkaline phosphatase (ALP) were tested according to the instruction manual. List of reagents (including catalog numbers) can be found in "Critical Commercial Assays" list.

Inflammatory cytokines test

For liver samples, the tissue was rinsed with pre-cold PBS to remove residual blood. Twenty mg of liver tissue was added to 200 μL PBS containing protease inhibitor PMSF, and further ground by tissue grinding instrument at 4°C. The homogenate was centrifuged at 5000 g for 10 min and the supernatant was collected for assay. The concentrations of proinflammatory factors (TNFα, IL-6, and IL-1β) from serum or liver samples were measured using ELISA according to the manufacturer's instructions.

Liver triglycerides examination

For the hepatic lipid extraction, each 12 mg of liver tissue was added to 500 μL extraction solvent mixed with chloroform: methanol (v: v = 2:1), homogenized by tissue grinding instrument, then fully shaken for 1 min, centrifuged at 4000 rpm at 4°C for 10 min, 10 μL supernatant were transferred into a clean centrifugal tube and dried at room temperature. Then, 10 μL pure water was added to the precipitates for redissolution. After adding with 200 μL working solution supplied by the TG test kit, the reaction mixture was incubated at 37°C for 10 min. After briefly vertexing, the absorbance at 510 nm was measured in 96-well plate. The concentration of TG was calculated according to the standard curve, and the results were presented as mmol/g liver weight.[84]

Tissues staining

Tissues were fixed with 10% formalin for over 24 h, embedded in paraffin, and then stained with hematoxylin-eosin staining (H&E) and Sirius Red using a standard protocol. Hematoxylin staining was used for nuclear counterstaining (blue), and eosin was used to stain the cytoplasm red. Sirius Red was used for collagen fibers staining (red). For Oil red O staining, fresh large lobes of the liver were embedded in OCT and flash-frozen in liquid nitrogen, then stored at −80°C. The embedded tissues were sectioned into 8 μm pieces after equilibrated at −20°C, and then stained with Oil red O to determine the extent of hepatic steatosis.

Histopathological evaluation

NAFLD activity score (NAS, 0 to 8) including separate scores for steatosis (0–3), lobular inflammation (0–3) and hepatocellular ballooning scale (0–2). The criteria for hepatic steatosis scoring include grade 0, steatosis involved <5%; grade 1, steatosis involved between 5 and 33%; grade 2, steatosis involved between 34 and 66%; and grade 3, steatosis involved >66%. Hepatic lobular inflammation was grade based on overall assessment of all inflammatory foci per 200 field, including grade 0, no foci; grade 1, <2 foci per 200 field; grade 2, 2–4 foci per 200 field; grade 3, >4 foci per 200 field. Ballooning degeneration was scored by the severity based on numbers of hepatocytes: 0 points assigned as none, 1 point as mild, 2 points as marked.[85]

Liver F4/80 and CD11b immunofluorescence staining

Tissue paraffin sections were permeabilized in PBS supplemented with 0.4% Triton X-100 (Sigma-Aldrich) and 3% BSA (Sigma-Aldrich) for 1 h and preincubated in blocking buffer (PBS supplemented with 3% BSA) for 1 h. Tissues were then labeled with anti-F4/80 or anti-CD11b primary antibody and the corresponding secondary antibody for 2 h at room temperature. Then, immunofluorescence imaging was performed.

Quantification of ^{13}C incorporated fatty acids

Flox and LKO mice (n = 6) were fed an AMLN diet for 7 days, fasted from 9 a.m. to 7 p.m., refed for 2 h, and force-fed ^{13}C-fructose. The mice were fed overnight and killed the next morning. LC-MS was performed to examine the amount of ^{13}C label incorporation into hepatic fatty acids.

Oil red O staining for cells

Cells were gently washed 2 times with PBS. 10% formalin was added to each well and incubated for 30 min. Then formalin was removed, and cells were gently washed 2 times with ddH_2O. Each well was added 60% isopropanol and incubated for 5 min. After removing isopropanol, Oil Red O working solution was added to cover the cells completely and evenly and incubated for 10–20 min, then cells were washed 2–5 times with ddH_2O as needed. Hematoxylin was added to the cells and incubated for 1 min, and washed 2–5 times as needed. Cells was viewed under microscope. Lipid droplets appear red and nucleal appear blue.[86]

Immunohistochemical staining and quantification

After deparaffinization and dehydration, antigen retrieval was performed using a microwave for 5 min, before peroxidase quenching with 3% H_2O_2 in phosphate-buffered saline (PBS) was done for 15 min. Subsequently, the sections were blocked with 5% bovine serum albumin (BSA) for 30 min and then incubated with a primary antibody at a dilution ratio of 1:500 in PBS overnight at 4°C. The negative control was treated in the same way, as were the sample groups, except that primary antibody were omitted in the incubation steps. The percentage of the area of the section occupied by positive staining was determined using ImageJ 1.53 software.

Immunofluorescence

For multiple immunofluorescence, Firstly, after washing twice with PBS, the cells were fixed in 4% paraformaldehyde in PBS for 15 min and then washed three times in PBS with Tween 20 (PBST). After removing supernatant, the PBS solution containing 0.5% Triton X-100 was used for permeation for 15–20 min. The permeation solution was discarded, PBS solution containing 5%

donkey serum was added to seal the cells at room temperature for 1h. After removing the blocking solution, a primary antibody diluted with 5% BSA and 0.1% Triton X-100 PBS solution (1:150 dilution) was added and incubated overnight at 4°C. The next day, cells were washed 3 times with PBST. Fluorescent secondary antibody was added (diluted with PBS solution containing 5% BSA, 1:200), and incubated for 1 h at room temperature in dark. After washing with PBST, the sealing solution containing Hoechst dye was added under dark conditions and stored at 4°C. Images was detected and captured by Fluorescent Confocal Microscopy (Leica, TCS SP-8, Germany). To generate three-dimensional images, images were recorded as vertical z stacks and processed using Leica LAS X 3.5.7 software.

Co-immunoprecipitation (Co-IP)

AML-12 cells were lysed with IP lysis buffer (P0013, Beyotime, China) containing an inhibitor cocktail. After centrifugation, the supernatant containing proteins was subjected to IP with protein G agarose beads (10007D, invitrogen, USA) and the indicated antibodies overnight at 4°C. The beads were washed with NaCl buffer and boiled with 2×SDS loading buffer prior to analysis by Western blotting.

Proximity ligation assay (PLA)

AML-12 cells were seeded on coverslips and allowed to attach overnight. After fixation in 4% paraformaldehyde, PLA was performed using Duolink *In Situ* Proximity Ligation Assay reagent (Sigma-Aldrich) according to the manufacturer's instructions. Briefly, blocking was performed with blocking solution for 30 min at 37°C, and primary antibodies: anti-SCAP(1:100 dilution), anti-SQSTM1(1:100 dilution), and anti-PKAc(1:100 dilution) were incubated overnight at 4°C. The PLA Probe anti-mouse MINUS and PLA Probe anti-rabbit PLUS were incubated for 1 h at 37°C. Ligation and amplification were performed using Detection Reagents Red. Duolink Mounting Medium with DAPI was used for nuclear staining and mounting. The average PLA signal intensity of each cell was calculated by ImageJ software.[87] List of reagents (including catalog numbers) can be found in "**Critical Commercial Assays**" list. List of antibodies can be found in "**Antibodies**" list.

Natural compound database screening

Natural compounds screening with activating capacity on A_1R activity was performed based on a commercial Natural Product Library Plus (website: https://www.medchemexpress.cn/screening/natural-product-library-plus.html) by using computer-aid molecular docking. The Virtual Screening Workflow module was used to perform virtual screening by importing the prepared compounds and using the Glide module to perform molecular docking, i.e., docking between receptor and ligand molecules by geometric and energy matching. The 3600 prepared small molecules in the Natural Product Library Plus were first screened using the High Throughput Screening (HTVS) mode in the Glide module, and the top 20% of the scored small molecules were selected for a second round of screening using the Standard (SP) mode; then the top 20% of the scored compounds were selected for a third round of screening using the High Precision (XP) mode to obtain the ranking of the small molecules. The top 200 compounds screened from Natural Product Library Plus, was further analyzed using cAMP test *in vitro*.

Protein isolation and western blot analyses

Tissue/Cells were lysed in RIPA Lysis Buffer (Beyotime, China) supplemented with PMSF (Beyotime, China) and protease inhibitors and phosphatase inhibitors (Sigma, USA). Nuclear or membrane extracts were prepared with a nuclear and cytoplasmic protein extraction kit (Beyotime, China) according to the manufacturer's instructions. Protein concentrations were measured with the BCA reagent (YEASEN, China) by using a Microplate Reader Spark System (TECAN, Switzerland). Equal amounts of protein were resolved by SDS–PAGE and immunoblotted with different antibodies as described previously. The immunoblots were detected using an Image 600 ECL System (GE, USA).

Extraction of total RNA and real-time quantitative PCR

Total RNA was isolated using an RNA purification kit (EZBioscience, USA), and then used to synthesize cDNA with the FastKing gDNA Dispelling RT SuperMix (TIANGEN, China). Real-time qPCR was performed using SYBR Green (Vazyme, China), 96-well plates and the CFX connect Real-Time System. Each well was loaded with a total of 20 μL containing 2 μL of cDNA, 0.5 μL of target primers, 7.5 μL of water and 10 μL of SYBR Select Master Mix. Real-time qPCR was performed for 40 cycles, with each cycle consisting of denaturation for 15 s at 94°C, annealing for 30 s at 60°C and elongation for 30 s at 72°C. Relative quantification was done using the $2^{-\Delta\Delta CT}$ method. Expression was normalized against *18s*. Mean expression levels of chow-fed mice were set as 100%. The primers used are shown below.

QUANTIFICATION AND STATISTICAL ANALYSIS

Data representation and statistical analysis

Data are presented as mean ± SEM (Standard Error of Mean). *p* values were obtained using unpaired Student's *t* test (between two groups) or One-way ANOVA analysis (during over two groups) for continuous variables via prism 9 (GraphPad Software Inc., La Jolla, CA). Significant differences among groups are indicated as *$p < 0.05$, **$p < 0.01$.

Cell Reports Medicine, Volume *5*

Supplemental information

Activation of hepatic adenosine A1 receptor ameliorates MASH via inhibiting SREBPs maturation

Weize Zhu, Ying Hong, Zhaowei Tong, Xiaofang He, Yan Li, Hao Wang, Xinxin Gao, Pengtao Song, Xianshan Zhang, Xiaochang Wu, Zhenhua Tan, Wenjin Huang, Zekun Liu, Yiyang Bao, Junli Ma, Ningning Zheng, Cen Xie, Xisong Ke, Wen Zhou, Wei Jia, Mingxiao Li, Jing Zhong, Lili Sheng, and Houkai Li

Activation of hepatic adenosine A1 receptor ameliorates MASH via inhibiting SREBPs maturation

Supplementary Figures

Fig S1

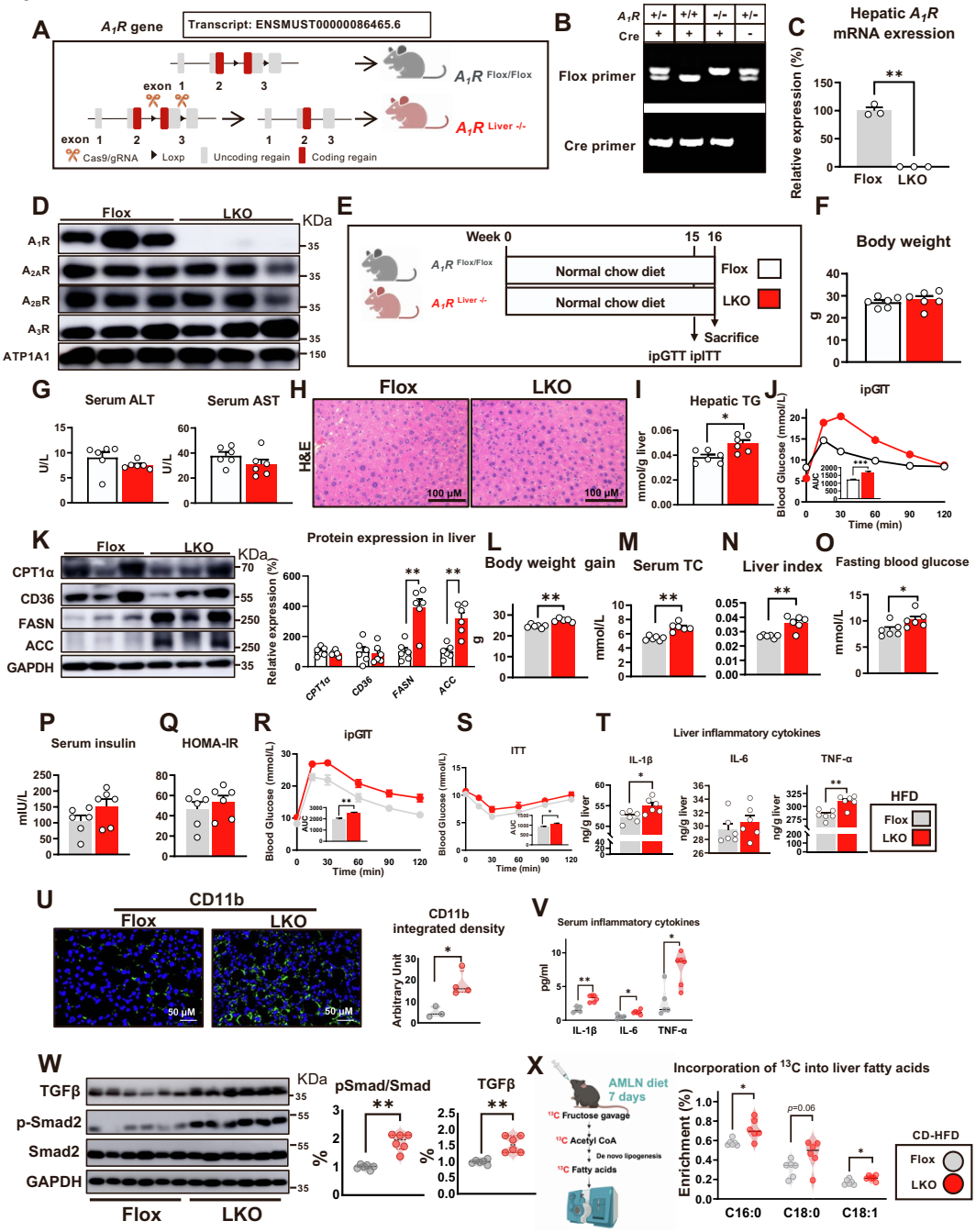

Fig. S1. Liver-specific A1R deletion exaggerates MAFL/MASH in mice. Related to Figure 1.
(**A**) Schematic showing the CRISPR-Cas9 technology targeting *A1R* to generate liver-specific knockout mice (LKO). (**B**) Agarose gel electrophoresis of qPCR amplification products from the mice with

various genotypes. (**C**) Hepatic *A_1R* mRNA expression from the Flox and LKO mice. (*n*=3) (**D**) The hepatocytes membrane proteins expression of adenosine receptor subtypes, including A_1R, $A_{2A}R$, $A_{2B}R$, and A_3R. Flox and LKO mice were fed with normal chow diet (ND) for 16 weeks (*n*=6). ATP1A1 was used as cytomembrane protein control. (**E**) Diagram of experimental design. (**F**) Body weight. (**G**) Serum ALT and AST. (**H**) the representative image of liver H&E staining. (**I**) Quantification of hepatic TG. (**J**) Blood glucose levels during ipGTT and corresponding AUC encompassing 120 min of ipGTT. (**K**) Relative protein expression of CPT1α, CD36, FASN, and ACC. GAPDH functioned as a reference protein. (**L** to **T**) Flox and LKO mice were fed with HFD for 16 weeks (*n*=5-6). (**L**) Body weight gain. (**M**) Serum total cholesterol. (**N**) Liver index (**O**) Fasting blood glucose level. (**P**) Fasting serum insulin level. (**Q**) HOMA-IR. (**R-S**) Blood glucose levels during ipGTT or ipITT and corresponding AUC. (**T**) Hepatic inflammatory cytokines including IL-1β, IL-6, and TNF-α. (**U-W**) Flox mice and LKO mice were fed a calorie-restricted HFD (CD-HFD) for 9 weeks (**U**) Immunofluorescence of CD11b in the liver of Flox and LKO mice. (*n*=3-4) (**V**) Serum inflammation cytokines including IL-1β, IL-6, and TNF-α. (*n*=5-6) (**W**) Relative protein expression of TGF-β, pSmad2, smad2. (*n*=6) (**X**) The enrichment of ^{13}C label incorporation into hepatic fatty acids were examined by LC-MS in Flox and LKO mice fed an AMLN diet for 7 days, fasted from 9 a.m. to 7 p.m., refed for 2 hours, and force-fed ^{13}C-fructose (*n*=6). Results are representative of 1 biological replicate. Data are depicted as mean ± SEM. Student's unpaired *t*-test; **p*<0.05, ***p*<0.01.

Fig S2

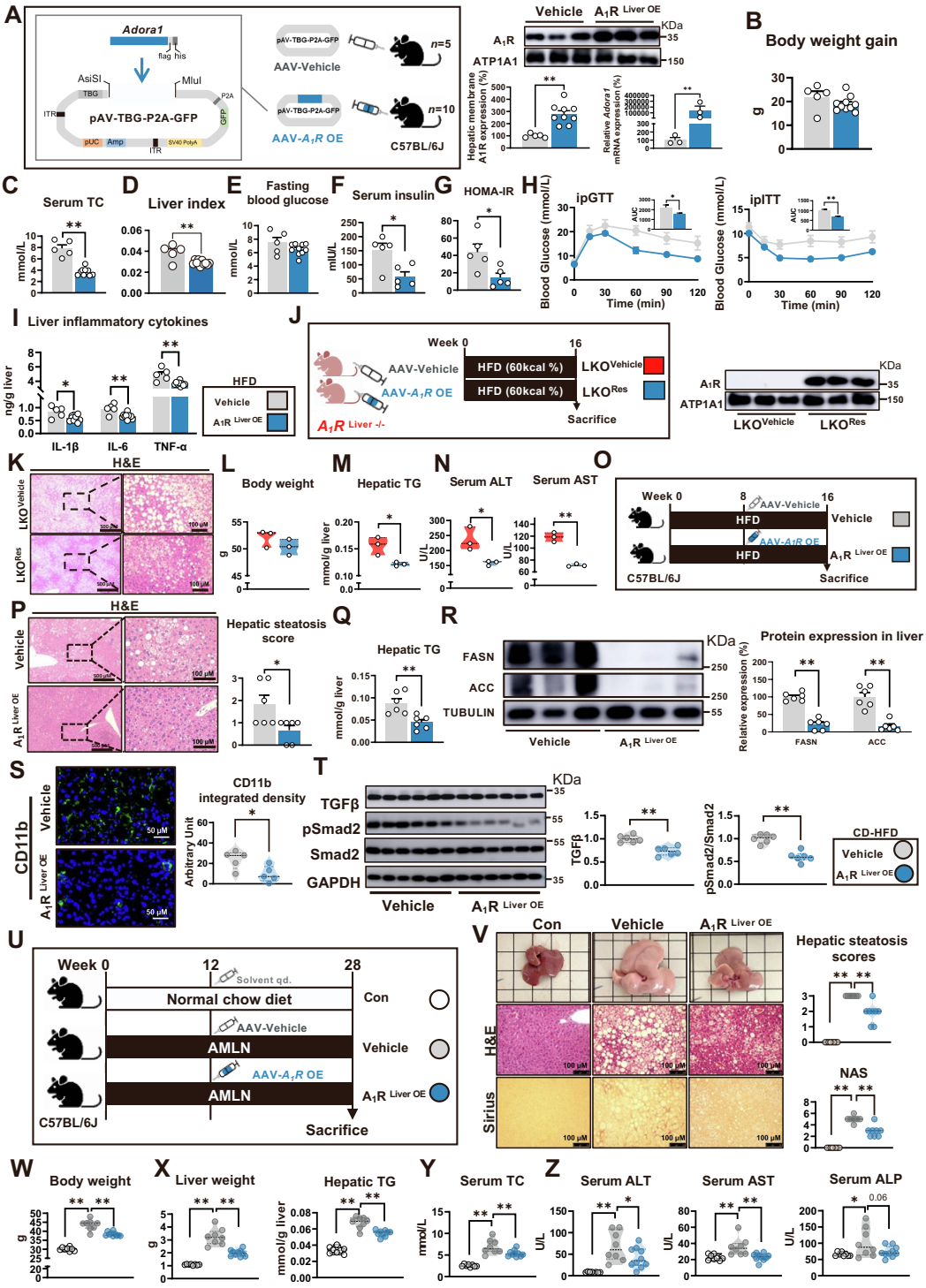

Fig. S2. Liver-specific A₁R overexpression protects mice from diet-induced NAFL/MASH. Related to Figure 2.

(**A-I**) C57BL/6J mice were inoculated with Vehicle-AAV (Vehicle) or *A1R*-overexpression-AAV (A1R $^{\text{Liver OE}}$) intravenously, and then were fed with HFD for 12 weeks (n=5~9). AAV, adeno-associated virus. (**A**) Schematic representation of construct AAV-mediated *A1R* overexpression mice, with A1R protein expression in cell membrane of hepatocytes and *Adora1* mRNA level. (**B**) Body weight gain. (**C**) Serum total cholesterol. (**D**) Liver index. (**E**) Fasting blood glucose level and (**F**) fasting serum insulin

level. (*n*=5) (**G**) HOMA-IR. (**H**) Blood glucose levels during ipGTT or ipITT and corresponding AUC. (**I**) Hepatic inflammatory cytokines including IL-1β, IL-6, and TNF-α. **(J-N)** LKO mice were inoculated with Vehicle-AAV ($LKO^{Vehicle}$) or *A1R*-overexpression-AAV (LKO^{Res}) intravenously, and then were fed with HFD for 16 weeks (*n*=3). (**J**) Diagram of experimental design, and A_1R protein expression in hepatic membrane. (**K**) The representative image of liver H&E staining. (**L**) Body weight. (**M**) Quantification of hepatic triglycerides (TG). (**N**) Serum alanine aminotransferase (ALT) and aspartate aminotransferase (AST). (**O-R**) Vehicle or *A1R*-overexpression-AAV ($A_1R^{\text{Liver OE}}$) intravenously at 9th week during 16 weeks HFD fed (*n*=6). (**O**) Diagram of experimental design. (**P**) The representative image of liver H&E staining, with hepatic steatosis score. (**Q**) Quantification of hepatic TG. (**R**) Relative protein expression of FASN, and ACC. (**S-T**) Vehicle mice and $A_1R^{\text{Liver OE}}$ mice were fed a CD-HFD for 9 weeks. (**S**) Immunofluorescence of CD11b in the liver of $A1R^{\text{Liver OE}}$ mice. (*n*=5) (**T**) Relative protein expression of TGF-β, pSmad2, smad2. (**U-Z**) Vehicle or $A_1R^{\text{Liver OE}}$ was intravenously injected at 13th week of the 28 weeks HFD feeding (*n*=8-10). (**U**) Diagram of experimental design. (**V**) Representative micrographs of liver, hepatic staining of H&E and Sirius red, along with Hepatic steatosis scores and NAS scores. (**W**) Body weight. (**X**) Liver weight and Quantification of hepatic TG. (**Y**) Serum TC level. (**Z**) Serum ALT, AST, and ALP. ATP1A1 was used as cytomembrane protein control. TUBULIN or GAPDH was used as total protein control. Results are representative of 1 biological replicate. Data are depicted as mean ± SEM. Student's unpaired *t*-test, One-way ANOVA analysis.; **p*<0.05, ***p*<0.01.

Fig S3

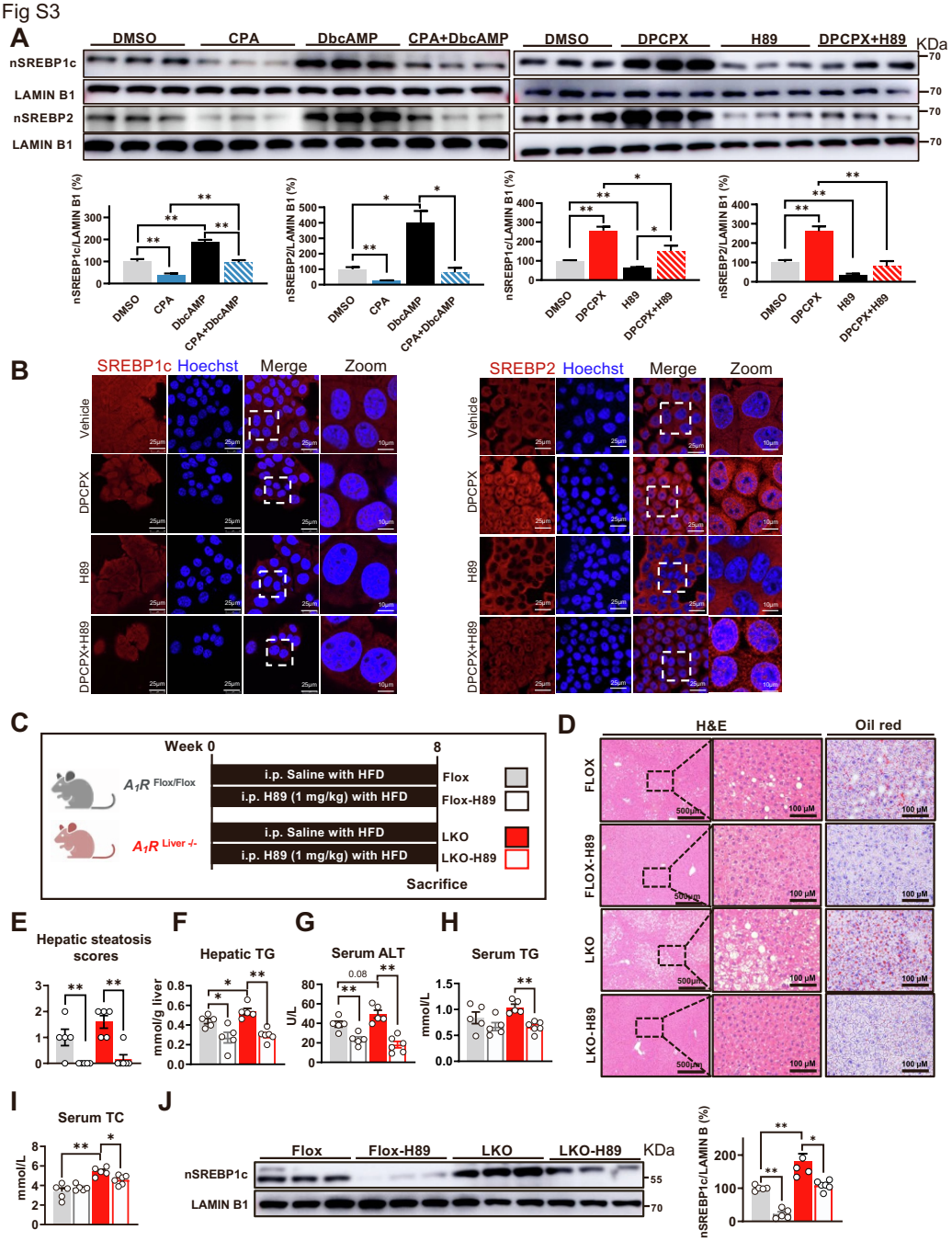

Fig. S3. A_1R controls the maturation of SREBPs via PKAc. Related to Figure 3.

(**A**) AML-12 cells were treated with CPA (A_1R activator, 1 μM, 48 h), DbcAMP (PKA activator, 200 μM, 12 h), DPCPX (A_1R inhibitor, 1 μM, 48 h), H89 (PKA inhibitor, 20 μM, 4 h), co-treated with CPA and DbcAMP, or co-treated with DPCPX and H89, respectively. nSREBP1c and nSREBP2 protein expression are shown. LAMIN B was used as nuclear protein control. (n=3) **(B)** AML-12 cells were treated with DPCPX (A_1R inhibitor, 1 μM, 48 h), H89 (PKA inhibitor, 20 μM, 4 h), or co-treated with DPCPX and H89, respectively. Fluorescent staining of SREBP1c or SREBP2 (red) in each group was performed. The nuclei were stained by hoechst (blue). **(C-J)** HFD-fed Flox and LKO mice were treated with or without H89 (i.p., 1 mg/kg body weight) daily for 8 weeks (n=5-6). (**C**) Diagram of experimental design. (**D**) The representative image of liver H&E and Oil red O staining, with hepatic

steatosis score. (**E**) Body weight. (**F**) Quantification of hepatic TG. (**G)** Serum ALT level. (**H**) Serum TG level. (**I**) Serum TC and LDL-C level. (**J**) Protein expression of nSREBP1c. LAMIN B1 was used as nuclear protein control. Results are representative of 1 biological replicate. Data are depicted as mean ± SEM. One-way ANOVA analysis; *p<0.05, **p<0.01.

Fig S4

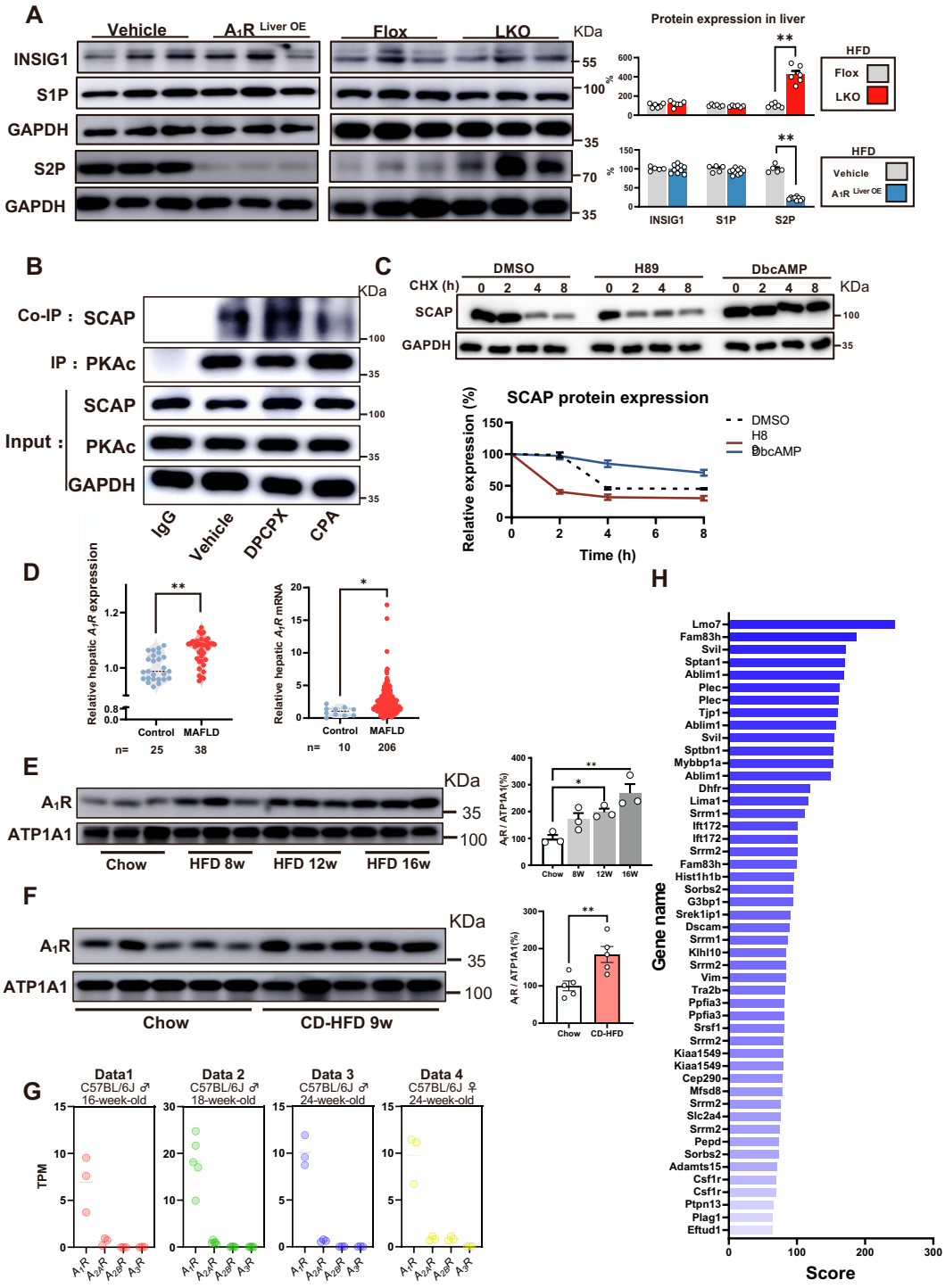

Fig. S4. A_1R activation accelerates SCAP protein degradation and hepatic A_1R expression is upgraded in MAFLD patients and mouse models. Related to Figure 3-6.

(A) Protein expression of INSIG1, S1P and S2P in liver of $A_1R^{\text{Liver OE}}$ (n=5-10) or LKO (n=6) mice. (**B**) Co-immunoprecipitation (co-IP) of PKAc with SCAP were performed in the AML-12 cells treated with DPCPX (1 μM) or CPA (1 μM) for 48 h. (**C**) Protein expression of SCAP in the AML-12 cells treated with H89 (20 μM, 4 h) or DbcAMP (200 μM, 12h) in the presence of cycloheximide (CHX, 50 μM) for 0, 2, 4, 8 h. GAPDH was used as total protein control. (n=3) **(D)** Gene and mRNA expression

of A_1R in liver of patient with MAFLD in public data (GSE89632, GSE135251). **(E-F)** A_1R protein expression in hepatocellular membrane of mice. (*n*=3-6) **(G)** mRNA expression of ARs in liver of mice. (*n*=3) ATP1A1 was used as cytomembrane protein control. (**H**) PKA-dependent phosphorylated targets in response to A_1R suppression. (Localization probability > 0.75; score diff >5 and score > 60). Results are representative of 1 biological replicate. Data are depicted as mean ± SEM. Student's unpaired *t*-test (A, D, F), One-way ANOVA analysis (G); **p*<0.05, ***p*<0.01.

Fig S5

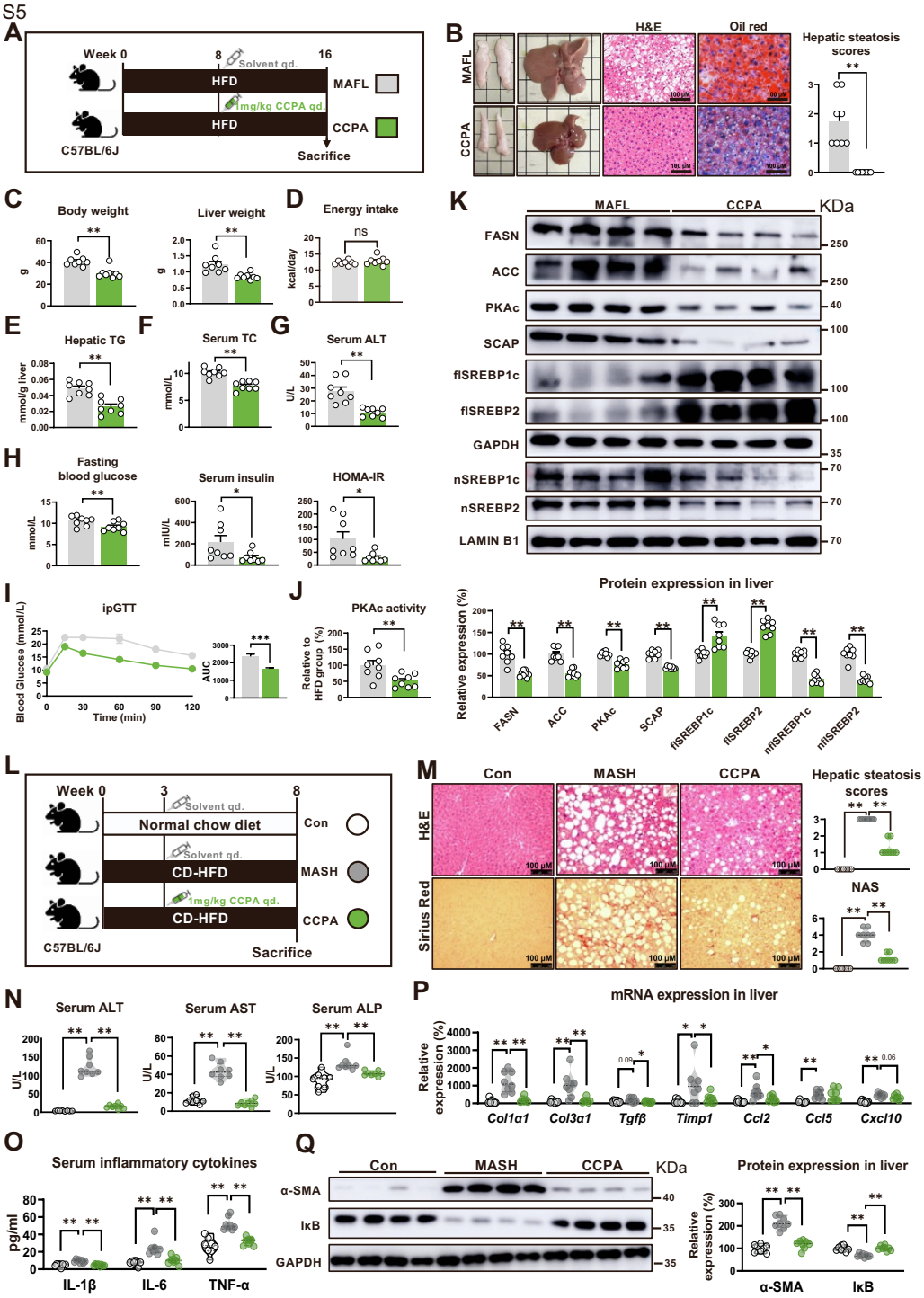

Figure S5. A_1R pharmacological activation inhibits diet-induced MAFL and MASH in mice. Related to Figure 7.

(**A** to **K**) C57BL/6J mice were fed a HFD for 16 weeks, and injected intraperitoneally 0.9% NaCl solution (NAFL) or 1 mg/kg 2-Chloro-N6-cyclopentyladenosine (CCPA) daily from 9th week. (*n*=8) (**A**) Diagram of experimental design. (**B**) Representative image of epididymis adipose, liver and liver staining of H&E and Oil red O, with hepatic steatosis scores. (**C**) Body weight and liver weight. (**D**) Energy intake (energy intake was record every week from 9th to 16th week, n=8 per group) (**E**) Quantification of hepatic TG. (**F**) Serum TC (**G**) Serum ALT. (**H**) Fasting blood glucose, serum insulin,

and HOMA-IR. (**I**) Blood glucose levels during ipGTT and corresponding AUC encompassing 120 min. (**J**) ELISA detection of active PKAc level. (**K**) Relative protein expression of PKAc, SCAP, SREBPs (flSREBP1c, flSREBP2, nSREBP1c, nSREBP2), and SREBP regulated proteins (FASN, ACC). GAPDH was used as total protein control, LAMIN B1 was used as nuclear protein control. (**L** to **Q**) C57BL/6J mice were fed a normal chow diet (Con) or CD-HFD for 9 weeks, during the process, CD-HFD mice were divided into 2 subgroups, and injected intraperitoneally 0.9% NaCl solution (CD-HFD) or 1 mg/kg CCPA daily from week 4. (n=8) (**L**) Diagram of experimental design. (**M**) H&E and Sirius red staining of liver sections, with histological evaluation. (**N**) Serum ALT, AST, and ALP. (**O**) Serum inflammatory cytokines including IL-1β, IL-6, and TNF-α. (**P**) mRNA expression of fibrosis-related genes (*Col1a1, Col3a1, Ctgf, Timp1*) and chemokine-related genes (*Ccl2, Ccl5, Cxcl10*) in liver. Results are normalized for *18S*. (**Q**) Relative protein expression of α-SMA and IκB. GAPDH was used as a control. LAMIN B1 was used as nuclear protein control. Results are representative of 1 biological replicate. Data are depicted as mean ± SEM. Student's unpaired *t*-test (**B** to **K**); One-way ANOVA analysis (**M** to **Q**); *p<0.05, **p<0.01.

Fig S6

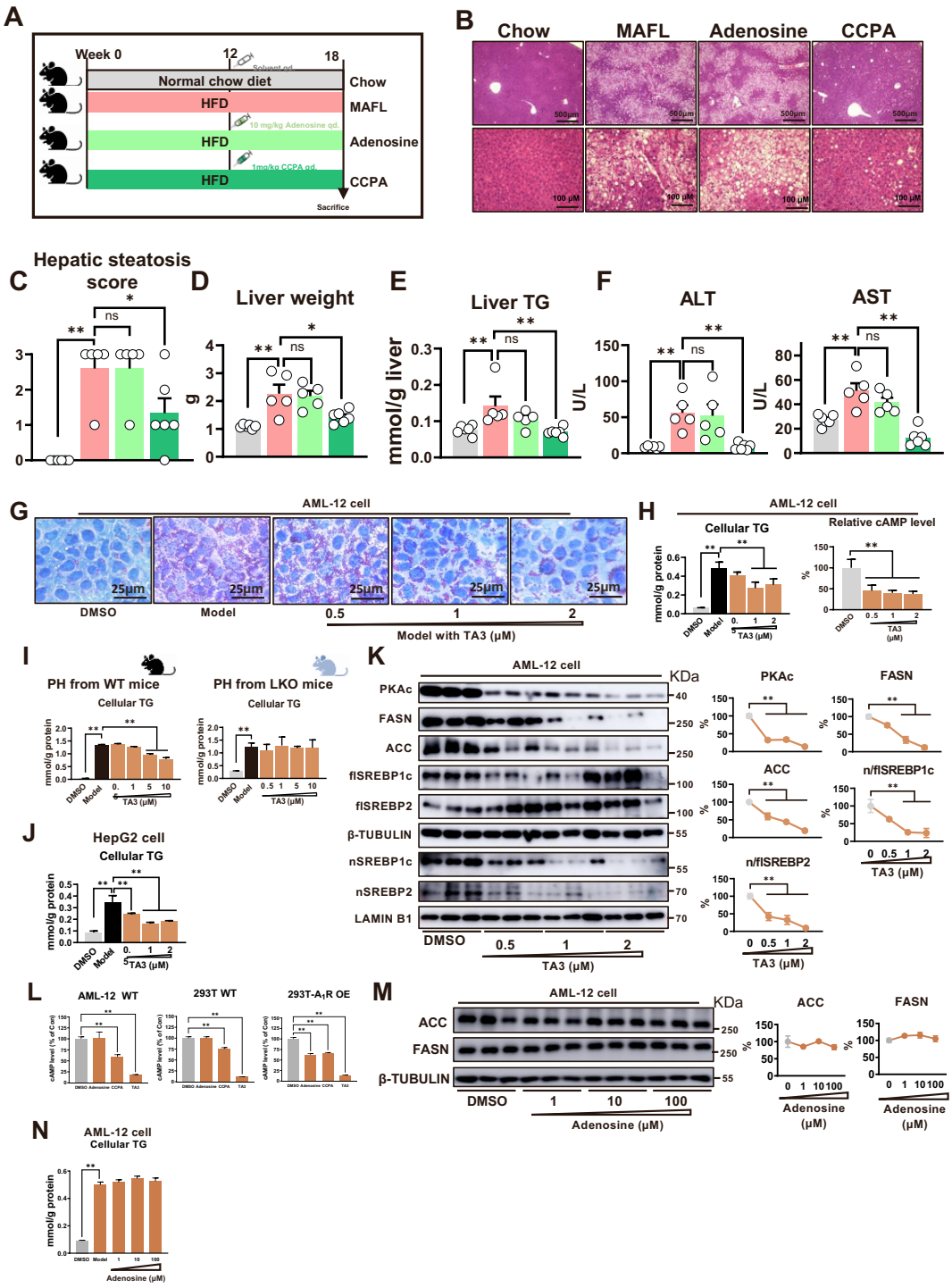

Figure S6. The anti-MAFLD test of Adenosine, and the screening and identification of A_1R activators. Related to Figure 7.

(**A** to **F**) C57BL/6J mice were fed a HFD for 18 weeks, and injected intraperitoneally 0.9% NaCl solution (NAFL) , 10mg/kg adenosine or 1 mg/kg 2-Chloro-N6-cyclopentyladenosine (CCPA) daily from 12th week. (n=5-6) (**A**) Diagram of experimental design. (**B**) Representative image of liver. (**C**) Hepatic steatosis score. (**D**) Liver weight. (**E**) Quantification of hepatic triglycerides (TG). (**F**) Liver injury indicators including serum alanine aminotransferase (ALT) and aspartate aminotransferase (AST). Results are representative of 1 biological replicate. Data are depicted as mean ± SEM. One-way

ANOVA analysis; n=5-6, *p<0.05, **p<0.01. (**G** to **N**) **The screening and identification of A_1R activators.** (**G-H**) AML-12 cells were treated with 0.5, 1, 2 μM timosaponin AIII (TA3) for 48 h in the presence of glycerol (20 mM) and glucose (4.5 g/L) (Model). Representative micrographs and the quantification of Oil Red O staining. Relative TG and cAMP level. (**I**) Cellular TG level in the primary hepatocytes (PH) from WT or LKO mice treated with 0.5, 1, 5, 10 μM TA3 for 48 h in the presence of glycerol (20 mM) and glucose (4.5 g/L) (Model). (**J**) Cellular TG level in HepG2 cells treated with 0.5, 1, 2 μM TA3 in model. (**K**) Relative protein expression of PKAc, SREBPs (flSREBP1c, flSREBP2, nSREBP1c, nSREBP2), and SREBP regulated proteins (FASN, ACC). (**L**) Cellular TG level. (**M**) Relative protein expression of FASN and ACC. (**N**) Cellular TG level. β-TUBULIN was used as total protein control; LAMIN B1 was used as nuclear protein control. Results are representative of 1 biological replicate, n=3. Data are depicted as mean ± SEM. One-way ANOVA analysis. *p<0.05, **p<0.01.

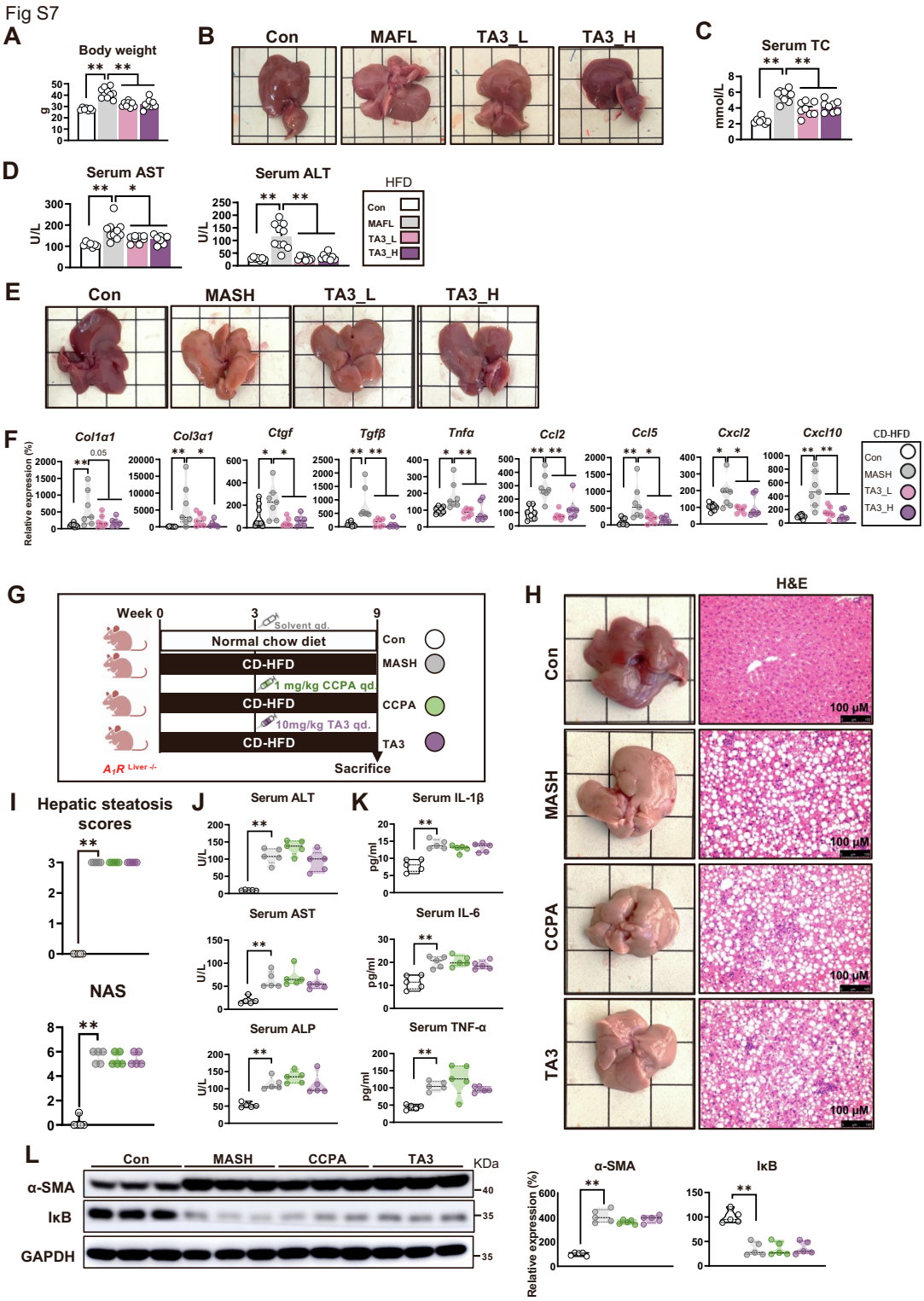

Figure S7. Timosaponin AIII inhibits diet-induced MAFL and MASH in mice in an A_1R-dependent manner. Related to Figure 7.

(**A** to **D**) C57BL/6J mice were fed with HFD for 16 weeks, and injected intraperitoneally 0.9% NaCl solution (HFD) or 5,10 mg/kg timosaponin AIII (TA3) daily from 9th week. (*n*=7-10) (**A**) Body weight. (**B**) Representative image of liver. (**C**) Serum TC. (**D**) Serum ALT and AST. (**E** to **F**) C57BL/6J mice were fed a normal chow diet (NCD, Con) or CD-HFD for 9 weeks, during the process, CD-HFD mice

were divided into 3 subgroups, and injected intraperitoneally with 0.9% NaCl solution (CD-HFD) or 5, 10 mg/kg TA3 daily from 4th week. (*n*=6-8) (**E**) Representative image of liver. (**F**) mRNA expression of fibrosis-related genes (*Col1a1, Col3a1, Ctgf, Tgfb*), proinflammatory-related genes (*Tnfα*), and chemokine-related genes (*Ccl2, Ccl5, Cxcl2, Cxcl10*) in liver of CD-HFD mice. (**G** to **L**) LKO mice were fed a normal chow diet or CD-HFD for 9 weeks, CD-HFD mice were injected intraperitoneally with 0.9% NaCl solution (MASH), 1 mg/kg 2-Chloro-N6-cyclopentyladenosine (CCPA) or 10 mg/kg TA3 daily from 4th week. (n=5) (**G**) Diagram of experimental design. (**H**) Representative image of Liver and hepatic H&E staining. (**I**) Histological evaluation. (**J**)Serum ALT, AST, and ALP. (**K**) Serum inflammatory cytokines. (**L**) Relative protein expression of α-SMA and IκB. GAPDH was used as total protein control. Results are representative of 1 biological replicate. Data are depicted as mean ± SEM. One-way ANOVA analysis; *p<0.05, **p<0.01. Results are normalized for *18S*. Results are representative of 1 biological replicate. Data are depicted as mean ± SEM. One-way ANOVA analysis; *p<0.05, **p<0.01.

Table S1. Clinical and biochemical characteristics of the patients with biopsy proven MAFLD. Related to Figure 6.

Characteristics	All (*n*=30)	MAFL (*n*=22)	Control (*n*=8)	*p* value
Demographics				
Age (years)	51.3±2.2	52.7±2.4	47.6±3.9	0.3116
Gender, n (%)				
Female	20 (64.1)	14 (63.6)	6 (75.0)	
Male	10 (35.9)	8 (36.4)	2 (25.0)	
BMI (kg/m^2)	22.1±0.7	22.5±0.9	20.9±0.6	0.3242
Biological data				
AST (U/L)	55.4±14.3	48.7±13.2	72.0±39.0	0.4719
ALT (U/L)	86.4±27.6	65.5±18.7	138.6±85.7	0.2386
Triglycerides (mmol/L)	1.61±0.26	1.90±0.34	0.96±0.17	0.0894
Total cholesterol (mmol/L)	4.08±0.21	4.23±0.26	3.75±0.37	0.3030
Glucose (mmol/L)	6.75±0.60	6.58±0.72	7.25±1.12	0.6361
Histology				
NAS, n (%)				
Steatosis				
0	8 (26.7)	0 (0.0)	8 (100.0)	
1	9 (30.0)	9 (40.9)	0 (0.0)	
2	10 (33.3)	10 (45.5)	0 (0.0)	
3	3 (10.0)	3 (13.6)	0 (0.0)	
Ballooning				
0	16 (53.3)	8 (36.4)	8 (100.0)	
1	14 (46.7)	14 (63.6)	0 (0.0)	
2	0 (0.0)	0 (0.0)	0 (0.0)	
Lobular Inflammation				
0	23 (76.7)	15 (68.2)	8 (100.0)	
1	7 (23.3)	7 (31.8)	0 (0.0)	
2	0 (0.0)	0 (0.0)	0 (0.0)	
3	0 (0.0)	0 (0.0)	0 (0.0)	
Fibrosis stage				
F0	30 (100.0)	22 (100.0)	8 (100.0)	
F1	0 (0.0)	0 (0.0)	0 (0.0)	
F2	0 (0.0)	0 (0.0)	0 (0.0)	
F3	0 (0.0)	0 (0.0)	0 (0.0)	
F4	0 (0.0)	0 (0.0)	0 (0.0)	
Clinical diagnose				
Hepatic hemangioma	15 (50.0)	12 (54.5)	3 (37.5)	
Liver traumatic rupture	7 (23.3)	2 (9.1)	5 (62.5)	
Hepatolithiasis	8 (26.7)	8 (36.4)	0 (0.0)	

Data are presented as mean ± SEM. *P* values were obtained using Student's *t*-test for continuous variables.

Table S2. Clinical and biochemical characteristics of the patients with biopsy proven MASH. Related to Figure 1.

Characteristics	All (*n*=13)	MASH (*n*=9)	Control (*n*=4)	*p* value
Demographics				
Age (years)	44.6±2.7	40.9±2.8	53.0±3.3	0.0287
Gender, n (%)				
Female	6 (46.2)	3 (33.3)	3(75.0)	
Male	7 (53.8)	6 (66.6)	1 (25.0)	
BMI (kg/m^2)	27.0±1.3	29.4±1.0	21.5±1.4	0.0007
Biological data				
AST (U/L)	62.6±10.6	70.8.0±12.5	44.3±19.3	0.2672
ALT (U/L)	99.5±19.1	126.3±20.8	39.2±19.6	0.0275
Triglycerides (mmol/L)	1.94±0.33	2.34±0.40	1.03±0.24	0.0631
Total cholesterol (mmol/L)	4.93±0.21	4.84±0.27	5.12±0.33	0.5499
Glucose (mmol/L)	5.45±0.27	5.62±0.38	5.06±0.14	0.3644
Histology				
NAS, n (%)				
Steatosis				
0	4 (30.8)	0 (0.0)	4 (100.0)	
1	2 (15.4)	2 (22.2)	0 (0.0)	
2	2 (15.4)	2 (22.2)	0 (0.0)	
3	5 (38.5)	5 (55.6)	0 (0.0)	
Ballooning				
0	4 (30.8)	0 (0.0)	4 (100)	
1	3 (23.1)	3 (33.3)	0 (0.0)	
2	6 (46.1)	6 (66.6)	0 (0.0)	
Lobular Inflammation				
0	4 (30.8)	0 (0.0)	4 (100)	
1	4 (30.8)	4 (44.4)	0 (0.0)	
2	2 (15.9)	2 (22.2)	0 (0.0)	
3	3 (23.1)	3 (33.3)	0 (0.0)	
Fibrosis stage				
F0	4 (30.8)	0 (0.0)	4 (100.0)	
F1	1 (7.7)	1 (11.1)	0 (0.0)	
F2	6 (46.1)	6 (66.7)	0 (0.0)	
F3	2 (15.4)	2 (22.2)	0 (0.0)	
F4	0 (0.0)	0 (0.0)	0 (0.0)	
Clinical diagnose				
MASH	9 (69.2)	9 (100.0)	0 (0.0)	
Hepatic hemangioma	3 (23.1)	0 (0.0)	3 (75.0)	
Hepatolithiasis	1 (7.7)	0 (0.0)	1 (25.0)	

Data are presented as mean ± SEM. *P* values were obtained using Student's *t*-test for continuous variables.

Table S3. Primers(mice) for qPCR.

REAGENT or RESOURCE	SOURCE	IDENTIFIER
Oligonucleotides		
18s forward: 5'-CCATCCAATCGGTAGTAGCG -3'	This paper	N/A
18s reverse: 5'-GTAACCCGTTGAACCCCATT-3'	This paper	N/A
A_1R forward: 5'-TGTGCCCGGAAATGTACTGG- 3'	This paper	N/A
A_1R reverse: 5'-TCTGTGGCCCAATGTTGATAAG-3'	This paper	N/A
Ccl2 forward: 5'-TACAAGAGGATCACCAGCAGC-3'	This paper	N/A
Ccl2 reverse: 5'-ACCTTAGGGCAGATGCAGTT-3'	This paper	N/A
Ccl5 forward: 5'-TGCTGCTTTGCCTACCTCTC-3'	This paper	N/A
Ccl5 reverse: 5'-TCTTCTCTGGGTTGGCACAC-3'	This paper	N/A
Cxcl10 forward: 5'-ATGACGGGCCAGTGAGAATG-3'	This paper	N/A
Cxcl10 reverse: 5'-ATGATCTCAACACGTGGGCA-3'	This paper	N/A
Cxcl2 forward: 5'-GCGCCCAGACAGAAGTCATA-3'	This paper	N/A
Cxcl2 reverse: 5'-CAGTTAGCCTTGCCTTTGTTCA-3'	This paper	N/A
Il6 forward: 5'-TAGTCCTTCCTACCCCAATTTCC-3'	This paper	N/A
Il6 reverse: 5'-TTGGTCCTTAGCCACTCCTTC-3'	This paper	N/A
Il1β forward: 5'-CCGTGGACCTTCCAGGATGA-3'	This paper	N/A
Il1β reverse: 5'-GGGAACGTCACACACCAGCA-3'	This paper	N/A
Tnfα forward: 5'-CATCTTCTCAAAATTCGAGTGACAA-3'	This paper	N/A
Tnfα reverse: 5'-TGGGAGTAGACAAGGTACAACCC-3'	This paper	N/A
Col1a1 forward: 5'-TGCTAACGTGGTTCGTGACCGT-3'	This paper	N/A
Col1a1 reverse: 5'-ACATCTTGAGGTCGCGGCATGT-3'	This paper	N/A
Col3a1 forward: 5'-ACGTAAGCACTGGTGGACAG-3'	This paper	N/A
Col3a1 reverse: 5'-CCGGCTGGAAAGAAGTCTGA-3'	This paper	N/A
Ctgf forward: 5'-TGACCCCTGCGACCCACA-3'	This paper	N/A
Ctgf reverse: 5'-TACACCGACCCACCGAAGACACAG-3'	This paper	N/A
Timp1 forward: 5'-GAGACCACCTTATACCAGCGTT-3'	This paper	N/A
Timp1 reverse: 5'-TACGCCAGGGAACCAAGAAG-3'	This paper	N/A
Actb forward: 5'-GTGACGTTGACATCCGTAAAGA-3'	This paper	N/A
Actb reverse: 5'-GCCGGACTCATCGTACTCC-3'	This paper	N/A